International Journal of Modern Physics B, Vol. 9, Nos. 18 & 19 (1995) 2321–2362


# FERROELECTRIC LIQUID CRYSTALS: FROM THE PLANE WAVE TO THE MULTISOLITON LIMIT

I. MUŠEVIČ, B. ŽEKŠ and R. BLINC
*J. Stefan Institute, Jamova 39, 61000 Ljubljana, Slovenia*

and

TH. RASING
*Research Institute for Materials and High Field Magnet Laboratory*
*University of Nijmegen, NL-6525 ED Nijmegen, The Netherlands*

In the presence of external fields or in restricted geometries, the originally continuous helical symmetry of the Sm C* phase is broken by the appearence of field- or geometry-induced soliton-like domain walls. As a result of this symmetry breaking, a crossover between the plane-wave-like and soliton-like regime occurs in both static and dynamic properties which is responsible for some remarkable phenomena such as field-induced optical biaxiality or a field-induced band structure of collective excitations. Whereas we find in the plane-wave-like regime a degenerate soft mode which splits below the Sm A→Sm C* transition into a symmetry recovering Goldstone-phason-mode and an amplitudon mode, we find in the soliton regime a splitting of the phason mode into acoustic and optic-like branches separated by a band gap. Within the same framework we also discuss other remarkable and extraordinary properties such as reentrant phases, Lifshitz points, one dimensional photonic band gaps and thickness dependent phase diagrams.

## 1. Introduction

In contrast to 3D periodic solids, many liquid crystalline phases exhibit a continuous rotational symmetry, which can be broken either spontaneously or by the presence of external fields or restricted geometries. This symmetry breaking is responsible for some remarkable thermodynamical properties of liquid crystals and is particular reflected in their dynamics, which is in many respects richer than the dynamics of solids. For instance, analogous to the case of many solid ferroelectrics, the ferroelectric Sm A→Sm C* phase transition is spontaneously induced by a doubly degenerate soft mode which softens in the Sm A phase on approaching $T_c$ until it freezes out at $T_c$. However, in contrast to solid ferroelectrics, a continuous rotational symmetry is broken at $T_c$ on going from the paraelectric Sm A phase to the ferroelectric Sm C* phase. In view of that, the doubly degenerate soft mode of the Sm A phase splits into two modes in the ferroelectric Sm C* phase: an amplitude mode which is analogous to the soft mode in solid ferroelectrics and a gapless symmetry recovering Goldstone mode. This Goldstone mode is responsible for the

intriguing optical, dielectric and thermodynamical properties of ferroelectric liquid crystals. In the presence of external fields or in a restricted geometry, the Goldstone mode splits into an acoustic-like branch and an optic-like branch, separated by a band gap. This splitting is the result of the change of the plane wave type helicoidal modulation of the Sm C* order parameter to a soliton-like modulation. Ferroelectric liquid crystals thus represent a unique system where the whole region from the plane-wave to the extreme narrow soliton type modulation regime can be induced at will and the corresponding dynamics studied.

Ferroelectric liquid crystalline materials undergo a second order phase transition from the higher-symmetry Sm A phase, where the molecules are oriented along the smectic normal, to the Sm C* phase, where the molecules are tilted with respect to the layer normal. This spontaneous tilting is accompanied by the appearance of a nonzero local spontaneous polarization in the plane of smectic layers, so that the Sm C* phase is a ***ferroelectric liquid crystalline phase.*** The orientational ordering of the long molecular axes is described by the equilibrium director field $\mathbf{n}_0(\mathbf{r})$, which in the Sm C* phase is tilted with respect to the layer normal at a tilt angle $\theta$, as shown in Fig. 1. The director $\mathbf{n}_0(\mathbf{r})$ precesses around the layer normal $\mathbf{e}_z$ as one moves from one layer to another and forms a helicoidal structure. This precession is slow on the molecular scale, so that the corresponding period $p_0$ of the helical structure is in the micrometer range. This is much larger than the length $l$ of liquid crystalline molecules,so that typically $l/p_0 \approx 10^{-3}$. The period of the helix is in

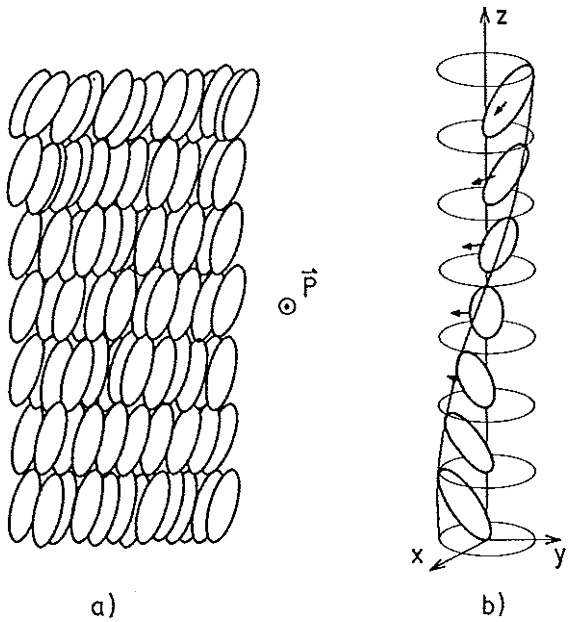


Fig. 1. Structure of the a) homogeneous and b) helicoidal Sm C* phase. The arrows in Fig. 1b illustrate the local orientation of the spontaneous polarization $\mathbf{P}(z)$.

principle incommensurate to the basic periodicity of the smectic layering. Because of the chirality of liquid crystalline molecules, the point symmetry of each smectic layer is $C_2$. This allows for the existance of a local electric polarization $\mathbf{P}_0(\mathbf{r})$ along the two-fold axis which is perpendicular to the plane of the tilt. The equilibrium polarization field $\mathbf{P}(\mathbf{r})$ thus precesses in the same way as the director field, so that the net electric dipole moment of the bulk Sm C* phase equals zero.

The Sm A→Sm C* phase transition is conveniently described within the Landau theory,[1] where the order parameter is the tilt of the molecules $\boldsymbol{\xi} = (\xi_x, \xi_y, 0)$

$$\xi_x = n_x n_z = \theta(z) \cos \Phi(z), \tag{1a}$$

$$\xi_y = n_y n_z = \theta(z) \sin \Phi(z). \tag{1b}$$

In the unperturbed Sm C* sample the magnitude of the tilt angle is constant, $\theta(z) = \text{const.}$, whereas the azimuth angle $\phi(z)$, which describes the slow precession of the director field $\mathbf{n}(z)$ as one moves along the $z$-direction, is linearly dependent on $z$ : $\Phi(z) = 2\pi z/p_0$.

The spontaneous tilting of the long molecular axis in the Sm C* phase is accompanied by the appearence of a spontaneous polarization $\mathbf{P}(z)$ along the local $C_2$ axis

$$P_x = -P_0 \sin \Phi(z), \tag{2a}$$

$$P_y = P_0 \cos \Phi(z). \tag{2b}$$

In contrast to proper ferroelectrics, where the spontaneous polarization is the primary order parameter,[2] the spontaneous polarization in ferroelectric liquid crystals is a secondary order parameter. This means that the Sm A→Sm C* phase transition is not driven by the interactions which originate from the dipole moments of individual molecules. Instead, the spontaneous polarization in ferroelectric liquid crystals is ***induced by the tilt***, which is here the primary order parameter, so that ferroelectric liquid crystals are improper, helicoidally modulated ferroelectrics.

The onset of the helicoidal ordering of molecules in the Sm C* phase of ferroelectric liquid crystals is responsible for some remarkable and extraordinary optical and thermodynamical properties of this phase. One can here observe and study many diverse and beautiful analogies to other systems such as incommensurate phases, spin waves, one-dimensional photonic band gaps, motion of a particle in a periodic potential, etc. In this respect, the Sm C* phase of ferroelectric liquid crystals represents a system where one can study rather general physical phenomena on a "mesoscopic", micrometer scale.

Recently, a significant progress in our understanding of thermodynamical properties and phase transitions in ferroelectric liquid crystals has been made. In particular, we have observed the underlying relations between the ***spontaneous symmetry breaking and symmetry breaking by external fields*** and their manifestation in the physical properties of ferroelectric liquid crystals. In this paper we would like to discuss in particular the similarities between a magnetic-field-induced and a

geometry-induced Lifshitz point and the relation between the symmetry breaking by external fields and the spectrum of collective excitations in ferroelectric liquid crystals. The paper begins with the introduction of the concept of the Lifshitz point, which has a physical realization in the $(H, T)$ phase diagram of a bulk ferroelectric liquid crystal in a transverse magnetic field $H$, and continues to the discussion of the phase diagram of a ferroelectric liquid crystal confined into a thin layer. This is, in our opinion, a good starting point for the understanding of phase behavior in complex structures of great current interest, such as gels and porous media. The paper then continues with the discussion of the optical properties of helical structures in external fields, where we use a simple perturbative approach to the optics of liquid crystals and show that the basic optical properties can be well described within such an approach. In Sec. 5 we introduce the concept of the order parameter excitations in the vicinity of the Sm A→Sm C* phase transition. After that, we discuss the effects of an external magnetic field on the spectrum of phason excitations and explain the observed phenomena on the basis of symmetry arguments. The paper concludes with the discussion of the quasielastic light scattering and the fundamentals of the optical detection of the linear electrooptical response in ferroeletric liquid crystals.

## 2. Lifshitz Point in Ferroelectric Liquid Crystals

The Lifshitz point, originally introduced by Hornreich, Luban and Shtrikman,[3] is a triple point where the disordered, homogeneously ordered and the inhomogeneously ordered phases coexist. The concept of a Lifshitz point was first introduced to the field of liquid crystals by A. Michelson[4] in the late 70's and represents a beautiful example of an analogy between liquid crystals and other spatially modulated systems. In his work, Michelson has considered the physical realization of a Lifshitz point in the $(H, T)$ phase diagram of a ferroelectric liquid crystal, where an external magnetic field is applied perpendicular to the helical axis.

If the diamagnetic anisotropy of liquid crystalline molecules is positive, molecules tend to align along the field direction. This results in the so-called ***soliton-like distortion*** of the helical structure, where long, almost uniformly aligned domains are separated by thin domain walls, where the director changes the orientation by 180° as we move along the helix. A 3D view of such a soliton-like distortion is shown in Fig. 2. The thickness of the domain walls decreases upon increasing field, whereas the period of the distorted structure increases. At a certain ***critical field*** $H_c$ the distorted helical structure unwinds into the spatially homogeneous Sm C structure, as shown in the $(H, T)$ phase diagram in Figs. 3a and 3b. On the other hand, if we ***decrease the temperature*** $T$ from the Sm A phase of a ferroelectric liquid crystal in a low external magnetic field, we will cross at a certain temperature the phase transition line $T_\lambda(H)$ and enter the modulated Sm C* phase. Alternatively, at high enough magnetic fields we will cross the phase transition line $T_0(H)$ and enter the spatially homogeneous Sm C phase, as shown in Fig. 3. The phase transition lines $T_\lambda(H)$, $T_0(H)$ and $H_c(T)$ thus merge into a single ***Lifshitz point*** $(H_L, T_L)$, where

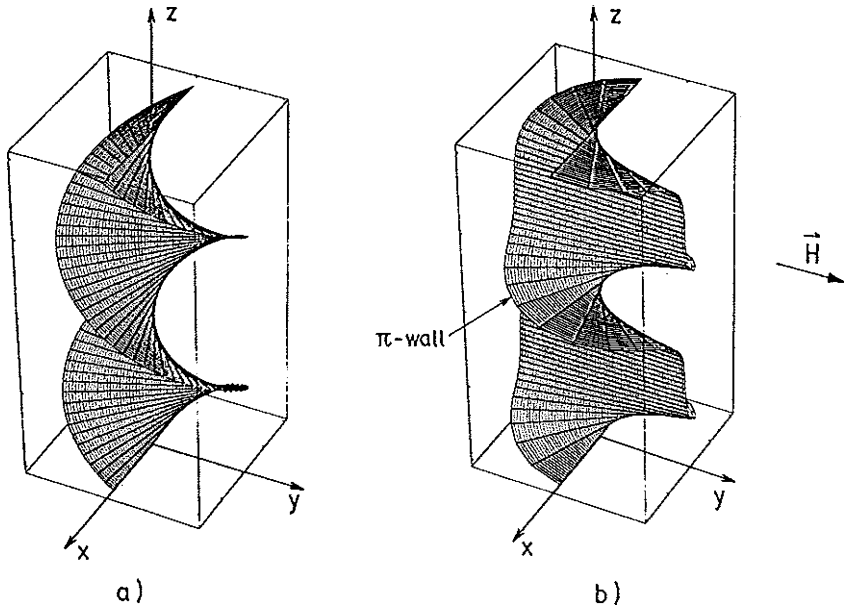


Fig. 2. Distortion of the helicoidal Sm C* structure by a transverse magnetic field. A 3D-view of the projection of the director field $\mathbf{n}(z)$ onto the smectic layers is shown for $H = 0$ (Fig. 2a) and $H \approx H_c$ (Fig. 2b), as calculated from the sine-Gordon equation (see Eqs. (13) and (14)). The $\pi$-soliton wall is indicated in b). Alternatively, Fig. 2a represents a surface with a continuous helical symmetry, like for example a uniformly twisted ribbon. Figure 2b represents a surface which has a discrete translational symmetry because of the $\pi$-soliton walls. One can consider it as a nonuniformly twisted ribbon, for example.

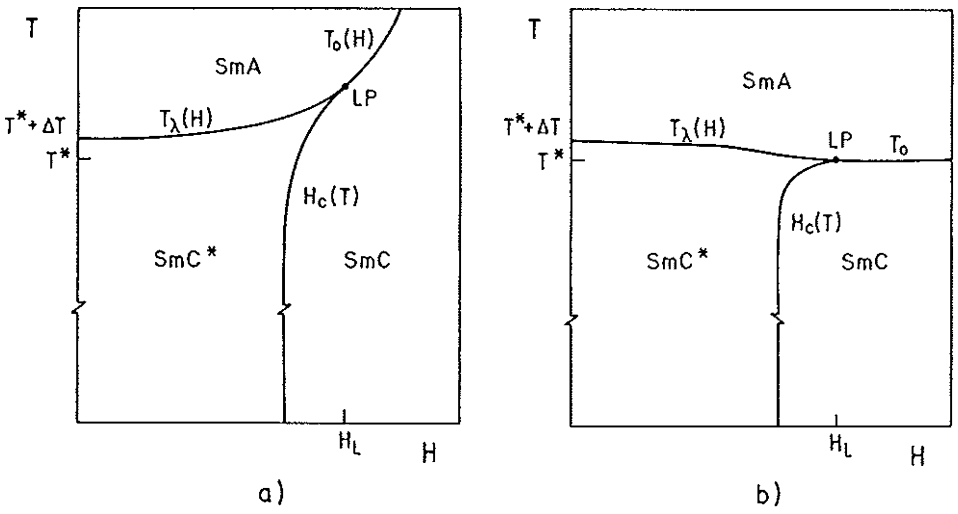


Fig. 3. Lifshitz point $(H_L, T_L)$ in the $(H,T)$ phase diagram of a ferroelectric liquid crystal in an external magnetic field for a) positive diamagnetic anisotropy and b) negative diamagnetic anisotropy. Both diagrams are schematic and $T^* = T_R^* + \frac{1}{\alpha}\epsilon C^2$, where $T_R^*$ is the phase transition temperature for the racemic mixture.

the disordered (Sm A), homogenerously ordered (Sm C) and helicoidally ordered (Sm C*) phases coexist.

Basic features of the ($H$, $T$) phase diagram of a ferroelectric liquid crystal in an external magnetic field can be derived from the simple Landau free-energy expansion[1,4]

$$g(z) = g_A + \frac{1}{2}a(T)\left(\xi_x^2 + \xi_y^2\right)^2 + \frac{1}{4}b\left(\xi_x^2 + \xi_y^2\right)^2 - \Lambda\left(\xi_x\frac{\partial\xi_y}{\partial z} - \xi_y\frac{\partial\xi_x}{\partial z}\right)$$
$$+ \frac{1}{2}K_3\left(\left(\frac{\partial\xi_x}{\partial z}\right)^2 + \left(\frac{\partial\xi_y}{\partial z}\right)^2\right) + \frac{1}{2\epsilon}\left(P_x^2 + P_y^2\right) - \mu\left(P_x\frac{\partial\xi_x}{\partial z} + P_y\frac{\partial\xi_y}{\partial z}\right)$$
$$+ C\left(P_x\xi_y - P_y\xi_x\right) - \frac{1}{2}\Delta\chi\, H^2\,\xi_2^2\,. \tag{3}$$

Here, $g_A$ is the equilibrium free-energy density of the Sm A phase, $\Delta\chi$ is the diamagnetic anisotropy and the magnetic field is applied in the $y$-direction, $\mathbf{H} = (0, H, 0)$. We assume that $a(T) = \alpha(T - T_R^*)$, $\alpha$ and $b$ are positive constants, and $T_R^*$ is the phase transition temperature for the racemic mixture. A racemix mixture is a 1:1 mixture of the right- and left-handed enantiomers of the liquid crystal. In the Eq. (3), $\Lambda$ is the coefficient of the Lifshitz term, which has the origin in the chirality of the molecules and induces helical modulation of the Sm C* phase, $K_3$ is the torsional elastic constant, $\epsilon$ is the dielectric constant of the Sm A phase, $\mu$ is the flexoelectric coefficient and $C$ is the electroclinic coefficient. We assume that the system is homogeneous in the $x$–$y$ plane, which is parallel to the smectic planes.

The polarization terms in the Eq. (3) can be eliminated by minimizing g($z$) with respect to $P_x$ and $P_y$. This results in the relation between the equilibrium spontaneous polarization **P** and the tilt vector $\boldsymbol{\xi}$

$$P_x = \epsilon\mu\frac{\partial\xi_x}{\partial z} - \epsilon C\,\xi_y \tag{4a}$$

$$P_y = \epsilon\mu\frac{\partial\xi_y}{\partial z} + \epsilon C\,\xi_x \tag{4b}$$

and renormalizes $K_3$, $\Lambda$ and $a(T)$,

$$\tilde{K}_3 = K_3 - \epsilon\mu^2\,, \qquad \tilde{\Lambda} = \Lambda + \epsilon\mu C\,, \qquad \tilde{a}(T) = a(T) - \epsilon C^2\,. \tag{5}$$

Note that the renormalization of $a \to \tilde{a}$ changes the phase transition temperature by $+\frac{\epsilon C^2}{\alpha}$. The partially minimized free-energy density is written as

$$g(z) = g_A + \frac{1}{2}\tilde{a}(T)\left(\xi_x^2 + \xi_y^2\right)^2 + \frac{1}{4}b\left(\xi_x^2 + \xi_y^2\right)^2 - \tilde{\Lambda}\left(\xi_x\frac{\partial\xi_y}{\partial z} - \xi_y\frac{\partial\xi_x}{\partial z}\right)$$
$$+ \frac{1}{2}\tilde{K}_{33}\left(\left(\frac{\partial\xi_x}{\partial z}\right)^2 + \left(\frac{\partial\xi_y}{\partial z}\right)^2\right) - \frac{1}{2}\Delta\chi\, H^2\xi_y^2\,. \tag{6}$$

The phase transition boundaries between the Sm A phase and the lower temperature modulated Sm C* or homogeneous Sm C can be obtained by the linear stability analysis.[4] As a result, one obtains the so-called ***Lifshitz field*** $H_L$

$$H_L = \frac{2\tilde{\Lambda}}{\sqrt{\tilde{K}_3 \mid \Delta\chi \mid}} \tag{7}$$

which characterizes the phase diagram and determines the position of the Lifshitz point in the $(H, T)$ phase diagram.

Below the Lifshitz field, $H < H_L$, the Sm A and the modulated Sm C* phases are separated by the $\lambda$-line, $T_\lambda(H)$

$$H \leq H_L : \quad T_\lambda(H) = T_R^* + \frac{1}{\alpha}\epsilon C^2 + \Delta T\left(1 + \frac{\Delta\chi}{\mid \Delta\chi \mid}\frac{H^2}{H_L^2}\right)^2 . \tag{8}$$

Here, $\Delta T = \frac{1}{\alpha}\frac{\tilde{\Lambda}^2}{\tilde{K}_3}$ describes magnetic-field dependence of the $\lambda$-line. For positive $\Delta\chi$ this line increases with the field, whereas for negative $\Delta\chi$ it decreases with the field. Along the $\lambda$-line the phase transition is of second order. Above the Lifshitz field, the Sm A phase transforms into the homogeneous Sm C phase at the second order phase boundary $T_0(H)$

$$H \geq H_L : \quad T_0(H) = T_R^* + \frac{1}{\alpha}\epsilon C^2 + 2\Delta T\left(1 + \frac{\Delta\chi}{\mid \Delta\chi \mid}\right)\frac{H^2}{H_L^2} . \tag{9}$$

The $(H, T)$ phase diagrams for the cases of positive and negative diamagnetic anisotropies and a simple Landau free-energy expansion (Eq. (3)) are shown schematically in Figs. 3a and b. Here, the most interesting feature is the position of the Lifshitz point $(H_L, T_L)$ in the phase diagram, which can be located by the Eqs. (7) and (8). It can be shown[4] that at the Lifshitz point the two phase boundaries $T_\lambda(H)$ and $T_0(H)$ merge tangentially to each other and to the line of the critical magnetic field $H_c(T)$ which separates the modulated and the unwound phase, as shown in Fig. 3. It can be also shown that near the Lifshitz point, the line of the critical magnetic field $H_c$ is of first order.[4]

Along the $\lambda$-line, the wave vector $q_c(H)$ of the modulated Sm C* phase decreases smoothly with the field

$$H \leq H_L : \qquad q_c(H) = q_c(0)\sqrt{1 - H^4/H_L^4} \tag{10}$$

from the value $q_c(0) = \frac{\tilde{\Lambda}}{\tilde{K}_3}$ at $H = 0$ to zero value at and above the Lifshitz field

$$H \geq H_L : \qquad q_c(H) = 0 . \tag{11}$$

The line of the critical field $H_c(T)$, which originates in the Lifshitz point and separates the modulated Sm C* and the homogeneous Sm C phase, can be derived

analytically only in the so-called constant amplitude approximation (CAA). Numerically, this line was first calculated by L. Benguigui and A. E. Jacobs.[5] Within the CAA one assumes that the magnitude of the tilt angles does not change significantly with the external field, whereas the phase $\Phi(z)$ is allowed to vary with $z$ and $H$. It can be shown that this is a reasonable approximation except within 10 mK around the Lifshitz point.[6] The phase dependent part of the free-energy density is

$$g(z) = -\tilde{\Lambda}\theta^2\frac{\partial\Phi(z)}{\partial z} + \frac{1}{2}\tilde{K}_3\theta^2\left(\frac{\partial\Phi(z)}{\partial z}\right)^2 - \frac{1}{2}\Delta\chi H^2\theta^2\sin^2\Phi(z). \tag{12}$$

After the Euler–Lagrange minimization of the free-energy $F = \int g(z)\,dz$ with respect to $\Phi(z)$ and $\partial\Phi(z)/\partial z$ we obtain the well-known sine-Gordon equation for $\Phi(z)$

$$\frac{d^2\Phi(z)}{dz^2} + \left(\frac{\Delta\chi H^2}{2\tilde{K}_3}\right)\sin 2\Phi(z) = 0. \tag{13}$$

The phase profiles $\Phi_0(z)$ which minimize the free-energy have the form of the so-called ***π-soliton lattice*** and are described by the Jacobi's elliptic functions

$$\sin\Phi_0 = \mathrm{sn}(u, k). \tag{14}$$

Here, $\mathrm{sn}(u, k)$ is the Jacobi elliptic sine of the reduced coordinate $u = z/(\xi k)$, where $\xi = \sqrt{\tilde{K}_3/(|\Delta\chi|H^2)}$ is the magnetic coherence length. The modulus $k$ of the Jacobi's elliptic function is defined by the equation

$$k = \frac{H}{H_c}E(k), \tag{15}$$

where $E(k)$ is the complete elliptic integral of the second kind and $H_c$ is the critical magnetic field for the unwinding of the helical structure

$$H_c = \pi^2\sqrt{\frac{\tilde{K}_3}{\Delta\chi}}\frac{1}{p_0}. \tag{16}$$

Within this approximation the critical field is inversely proportional to the period $p_0$ of the unperturbed helix, which is similar to the behavior of chiral nematics in an external magnetic field.[7] The critical magnetic field is here temperature independent because the period of the unperturbed helix is temperature independent within the free-energy expansion (3).

The phase profile $\Phi_0(z)$ which satisfies the sine-Gordon equation is shown schematically in Fig. 4 for different magnetic fields. For $H = 0$ the helical modulation is plane-wave-like with a linear dependence of the equilibrium phase, $\Phi_0(z) = (2\pi/p_0)z$. For $H \neq 0$ the helical modulation changes into the soliton-like, which is most pronounced in the narrow-soliton regime near $H_c$, as shown in Fig. 4. Large regions of nearly constant phase, where the molecules are almost homogenously

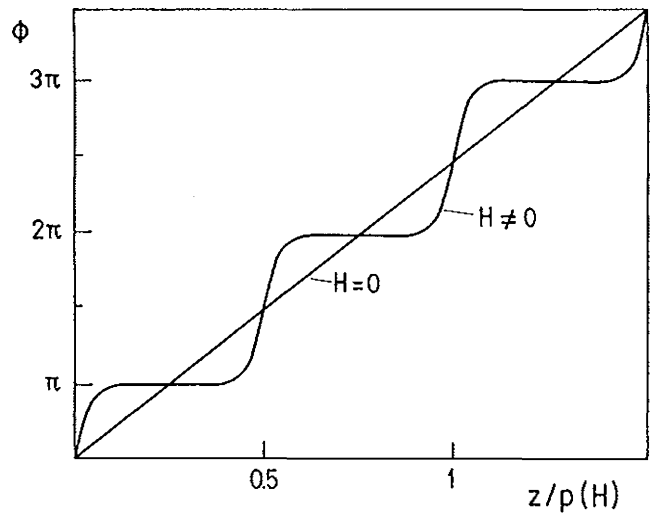


Fig. 4. The phase profiles $\Phi_0(z)$ which are the solutions of the sine-Gordon equation for $H = 0$ and $H \neq 0$. The figure is schematic and illustrates the appearance of the $\pi$-soliton walls, where the phase changes by 180° on a very short distance.

aligned into the field direction, are separated by narrow $\pi$-soliton walls. Within the soliton wall the phase $\Phi_0$ changes by 180° on a very short distance. By decreasing the magnetic field, the width of the soliton walls decreases slightly, whereas the distance between the soliton walls increases and diverges at $H_c$. The phase transition is here of second order with the divergence of the helical period

$$p(H) = p_0 \left(\frac{2}{\pi}\right)^2 K(k)\, E(k)\,. \tag{17}$$

Here, $K(k)$ is the elliptic integral of the first kind which diverges logarithmically at $H_c$.

In Eq. (8), $\Delta T = \frac{1}{\alpha} \frac{\tilde{\Lambda}^2}{\tilde{K}_3}$ determines the magnitude of the increase of the phase transition temperature $T_\lambda$ at the Lifshitz point. Typically, $\alpha \approx 10^4$ $\mathrm{Nm^{-2}K^{-1}}$, $\tilde{\Lambda} \approx 10^{-5}$ $\mathrm{Nm^{-1}}$ and $\tilde{K}_3 \approx 10^{-12}$ N, so that the expected increase of the phase transition temperature is of the order of $\Delta T \approx 10$ mK for a ferroelectric liquid crystal with a period of the helix of $p_0 \approx 1$ $\mu$m. The magnitude of the Lifshitz field can be estimated from Eq. (7). By taking $\mid \Delta\chi \mid \approx 10^{-6}$ one obtains $H_L \approx 15$ T, which is within the experimentally accessible range of static magnetic fields. In fact, the magnitude of the Lifshitz field can be adjusted by mixing different parts of the left- and right-handed enantiomers, thus changing the magnitude of the Lifshitz coefficient $\tilde{\Lambda}$ in Eq. (7).

The $(H, T)$ phase diagram of a ferroelectric liquid crystal in an external field was reported for the first time in high-magnetic filed experiments on p-decyloxybenzili-

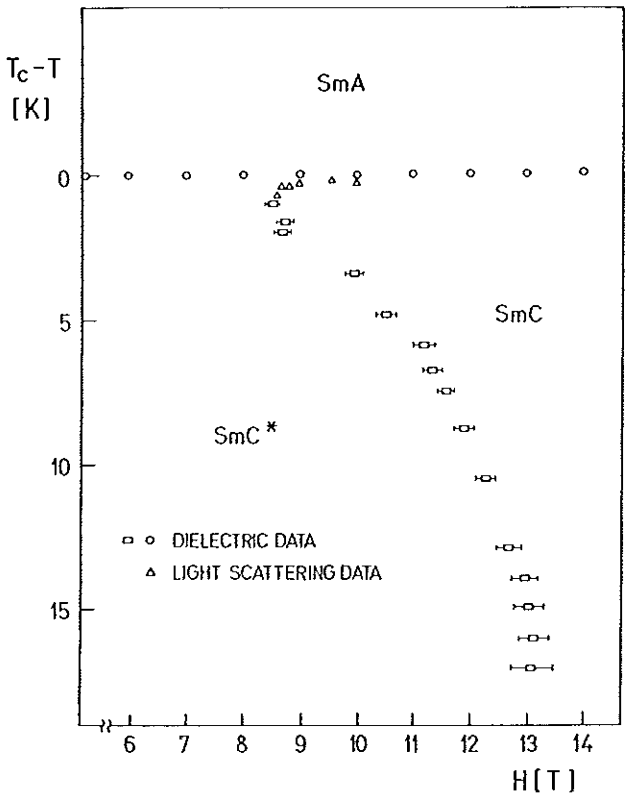


Fig. 5. $(H, T)$ phase diagram of a ferroelectric liquid crystal p-decyloxybenzilidene-p'-amino-2-methylbutyl cinnamate (DOBAMBC)[8] in an external magnetic field.

dene-p'-amino-2-methylbutyl cinnamate (DOBAMBC)[8] and is shown in Fig. 5. The phase boundaries were determined by light scattering and dielectric spectroscopy and are in qualitative agreement with theoretical predictions. The Sm A→Sm C* phase transition line was found to be practically field-independent within the resolution of 20 mK up to 10 T, which is in agreement with the estimated increase of the $\lambda$-line. Later on, the experimental work on the $(H, T)$ phase diagram was continued by A. Seppen,[9] who succeeded in observing the Lifshitz point in a mixture of chiral and racemic DOBAMBC. Recently, similar experiments were performed in the presence of a high frequency electric field,[10] which couples quadratically to the dielectric anisotropy.

The magnetic field experiment in chiral DOBAMBC, however, revealed for the first time the existence of a ***reentrant Sm C* phase*** very near the $\lambda$-line and indicated the "runaway" of the Lifshitz point in chiral DOBAMBC. Similar behavior was observed in recent electric-field experiments.[10] Furthermore, the experiment clearly showed a very strong temperature dependence of the critical field $H_c(T)$, which is in apparent disagreement with the predictions of a simple Landau model.

This peculiar behavior was explained by a high-resolution measurements of the temperature dependence of the period of the helix, which confirmed that the critical magnetic field is inversely proportional to the period of the helix,[9] $H_c(T) \propto \frac{1}{p_0(T)}$.

The observation of a strong temperature dependence of the critical magnetic field thus addressed the question of the relevance of a simple Landau model and the reasons for its apparent failure to describe magnetic-field effects correctly. The key question that any proposed model should answer seems to be the temperature dependence of the period of the helix in ferroelectric liquid crystals, which shows in many cases very characteristic and anomalous behavior in the vicinity of the Sm A→Sm C* transition.[11] Because of the relation (Eq. (16)) between the helical period and the critical magnetic field, this may reflect in the non-monotonous temperature dependence of the critical field and seems be the reason for the observed reentrance of the Sm C* phase in the $(H, T)$ phase diagram. There are several models which can explain this reentrance.[5,6] Among them, the so-called generalized Landau model,[6] as first introduced by Žekš in 1984,[12] seems to give the most complete description of most thermodynamic properties of ferroelectric liquid crystals[6,13] in a transparent and coherent fashion.

## 3. Phase Diagram of a Ferroelectric Liquid Crystal in a Restricted Geometry

Behavior of liquid crystals in restricted geometries is a subject of growing current interest because of important technological implications[14] as well as fundamental physics.[15,16] From the technological point of view, almost every liquid crystalline based device is a realization of a restricted geometry, where the liquid crystalline material is constrained to a thin spacing between two supporting glass plates. The ordering of the liquid crystal in such a geometry is determined by the liquid crystal-surface interaction and is obviously an important technological point. On the other hand, the liquid crystal-surface interaction is interesting from a fundamental point of view, because many interesting analogies to other systems can be studied. For example, if the surface coupling is a random variable in the interface plane, it will play the role of a random field, which strongly couples to the director field $\mathbf{n}(\mathbf{r})$ at the surface. This may have a very interesting influence on the order parameter dynamics as well as the nature of the phase transitions in liquid crystals. For nematic liquid crystals, some interesting studies have been published that used a very sensitive ellipsometry system to study the ordering at the liquid crystal-glass interface.[17]

Here we shall consider a simple example of a homogeneous surface coupling in a restricted geometry which has been studied previously.[18] The ferroelectric liquid crystal in the so-called bookshelf geometry is confined in between the two parallel plates, separated by a distance $d = 2L$, as shown in the inset to Fig. 6. The surface anchoring energy is taken into account in a simple form

$$g_s = \left[\delta(x + L) + \delta(x - L)\right] \frac{1}{2} C_s \xi_x^2 \tag{18}$$

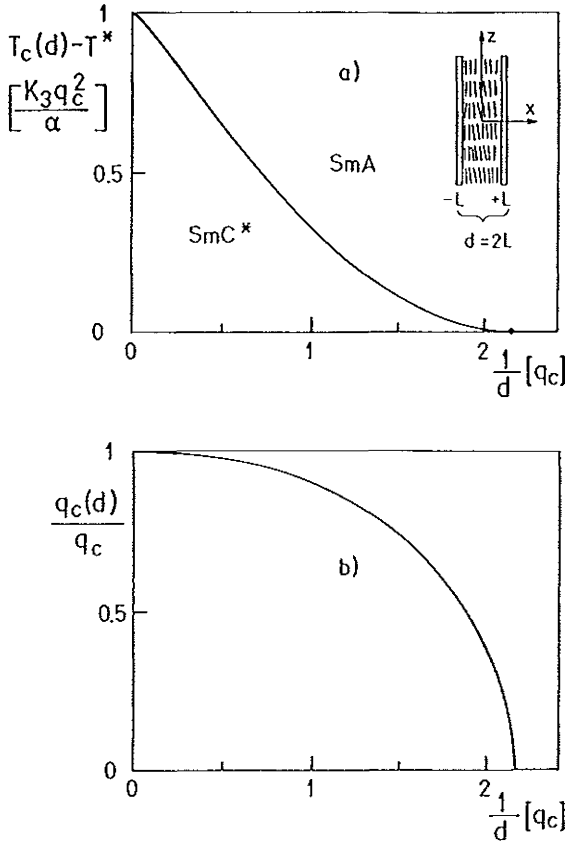


Fig. 6. The variation of the a) Sm A→Sm C* phase transition temperature $T_c(d)$ and b) critical wave-vector $q_c(d)$ along the $\lambda$-line. Here, $q_c$ is the wave-vector of the unperturbed Sm C* phase and $T^* = T_R^* + \frac{1}{\alpha}\epsilon C^2$, where $T_R^*$ is the phase transition temperature for the racemic mixture.

and $C_s$ is assumed to be constant throughout the interface. Here, $\xi_x$ is the out-of-plane component of the tilt and for a positive value of the coupling constant, $C_s > 0$, parallel alignment of $\xi$ with respect to the interface is favored. The homogeneous form of the surface anchoring energy in the $z$–$y$ plane, which favors homogeneous alignment, is competing with the "bulk" elastic energy, which favors helicoidal ordering far from the surfaces. For a thin enough sample we may thus expect that the helical structure would be unwound by the surface influence. In a certain way, the role of the surface term is thus similar to the role of the homogeneous magnetic or electric fields, which tend to unwind the helical Sm C* structure. We can thus expect that the $(d, T)$ phase diagram of a ferroelectric liquid crystal would resemble the $(H, T)$ phase diagram because of similar couplings.

The phase boundaries in the $(d, T)$ phase diagram of a ferroelectric liquid crystal can be determined by the stability analysis of the Sm A phase using the free energy

density

$$g(x,z) = \frac{1}{2}a(T)\left(\xi_x^2 + \xi_y^2\right) - \Lambda\left(\xi_x \frac{d\xi_y}{dz} - \xi_y \frac{d\xi_x}{dz}\right) + \frac{1}{2}K_3\left(\left(\frac{d\xi_x}{dx}\right)^2 + \left(\frac{d\xi_y}{dx}\right)^2\right)$$
$$+ \frac{1}{2}K_3\left(\left(\frac{d\xi_x}{dz}\right)^2 + \left(\frac{d\xi_y}{dz}\right)^2\right) + [\delta(x+L) + \delta(x-L)]\frac{1}{2}C_s\,\xi_x^2 . \qquad (19)$$

For the sake of simplicity we have been using here the old notation for $\Lambda$ and $K_3$, but one has to be aware that these are polarization-renormalized values. We have also used the one constant approximation for the elastic distortion in the $x$ and $z$ directions, respectively. The Sm A–Sm C* transition for an unconfined bulk sample is $T_c = T^* + \frac{1}{\alpha}K_3 q_c^2$, where $q_c = \Lambda/K_3$ is the wave vector of the undeformed helix and $T^* = T_R^* + \frac{1}{\alpha}\epsilon C^2$.

From Eq. (19) the stability analysis leads to a system of Euler–Lagrange equations for the bulk and surface, which can be solved by the ansatz

$$\xi_x(x,z) = f(x)\cos(qz), \qquad (20a)$$

$$\xi_y(x,z) = g(x)\sin(qz). \qquad (20b)$$

As a result,[19] one obtains a thickness dependent phase transition temperature $T_c(d)$, which is shown in Fig. 6a, together with the thickness dependence of the critical wave-vector $q_c(d)$ along this phase transition boundary, shown in Fig. 6b. Because the boundary conditions interfere with the helicoidal ordering, characterized by the wave-vector $q_c(d)$ in the Sm C* phase, for finite $d$ the phase transition Sm A→Sm C* will take place at a lower temperature than in the bulk. There will be, however, some limiting thickness $d_{LP}$, below which the phase transition Sm A→Sm C will take place. Since the homogeneous boundary conditions for $d < d_{LP}$ ***do not interfere*** with the homogenous ordering of the surface-unwound Sm C* phase, we expect a thickness-independent phase transition boundary for $d < d_{LP}$

$$d < d_{LP} \;:\quad T_c(d) = T^* = \text{const.}, \qquad (21)$$

$$d > d_{LP} \;:\quad T_c(d) < T_c(d \to \infty). \qquad (22)$$

The predicted ($d$, $T$) phase diagram thus resembles the ($H$, $T$) phase diagram of a ferroelectric liquid crystal with negative diamagnetic anisotropy, as shown in Fig. 3b. Furthermore, one can see from Fig. 6b that the critical wave-vector $q_c(d)$ goes ***continuously*** to zero at $d_{LP}$, which is thus a ***Lifshitz thickness***, where the Sm A, distorted Sm C* phase and the homogeneous Sm C phases coexist. The value of the Lifshitz thickness depends on the surface coupling constant and the liquid crystalline material constants, and can be evaluated in the limiting cases of weak

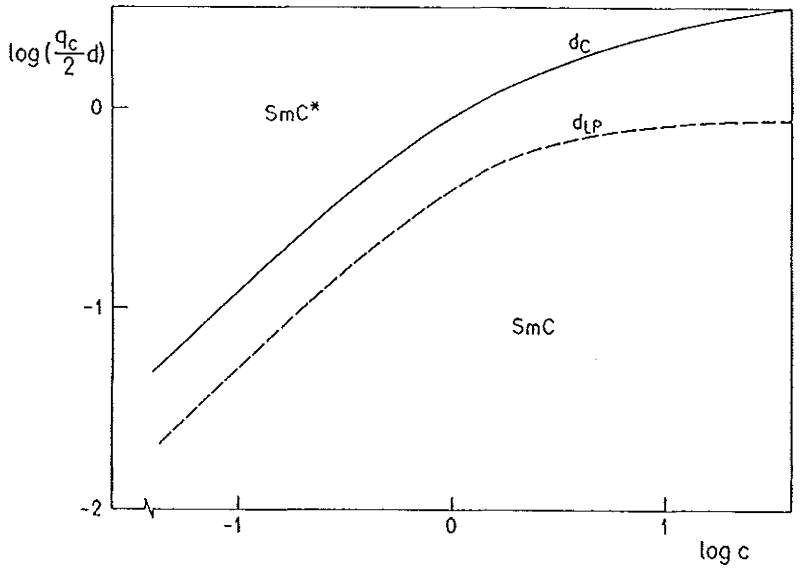


Fig. 7. The variation of the Lifshitz thickness $d_{LP}$ and the critical thickness $d_c$ with the normalized surface coupling strength $c = \frac{C_s}{2K_3 q_c}$.

and strong surface anchoring couplings, respectively,

$$C_s \to 0\,, \quad d_{LP} \to 0\,, \tag{23a}$$

$$C_s \to \infty\,, \quad d_{LP} \to \frac{\sqrt{3}}{2\pi} p_0 = 0.276\, p_0\,. \tag{23b}$$

The phase transition boundary between the distorted Sm C* phase and the surface unwound Sm C phase can be treated analogously to the cholesteric–nematic transition.[20] In the constant amplitude approximation the Sm C* → Sm C phase transition is of second order at a critical thickness $d_c$. The analysis gives the variation of the critical cell spacing $d_c$ with the anchoring strength $C_s$, which is illustrated in Fig. 7 together with the corresponding Lifshitz thickness $d_{LP}$. For small anchoring strengths, the ratio between $d_c$ and $d_{LP}$ is constant, which is similar to the critical magnetic fields in the $(H, T)$ phase diagram. However, in the limit of strong surface anchoring the situation is quite different. Whereas the Lifshitz thickness saturates for large $C_s$, this seems not to be the case with $d_c$. Instead, the critical thickness continues to grow with increasing $C_s$. This is a strong indication that the constant amplitude approximation is valid at small $C_s$, but breaks down at large $C_s$. Experimental observations of the Sm C* structures in thin samples[21] indicate that instead of a continuous director field, a system of disclination lines mediates the transition between the homogeneous orientation dictated by the surface and the helical structure in the interior of the liquid crystal. This means that we are always in the strong coupling regime. In the case of a system of disclination

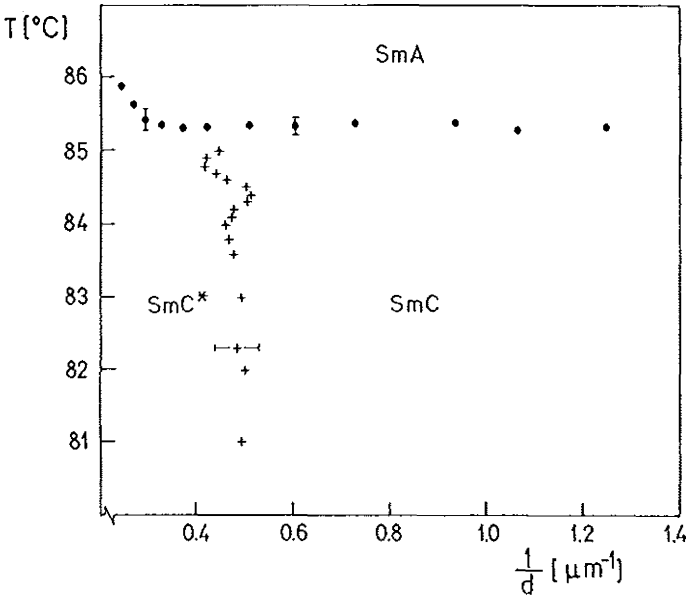


Fig. 8. $(d, T)$ phase diagram of CE-8 on polyimide PIX-1400 surface.

lines, the critical thickness is[19]

$$d_c = \frac{p_0}{2}\sqrt{\frac{K_1}{K_3}}. \tag{24}$$

Here, $K_1$ is the elastic constant for bend deformation, which is assumed to be equal to the splay elastic constant.[19,21] The $(d, T)$ phase diagram has been determined in wedge type cells of liquid crystal 4-(2'-methylbutyl) phenyl 4'-n-octylbiphenyl-4-carboxylate (CE-8), using untreated polyimide coated surfaces.[19] The observed phase diagram is shown in Fig. 8 and is in qualitative agreement with theory. The critical thickness is 2 $\mu$m at $T_c - T = 5\,\mathrm{K}$ and increases slightly on approaching the Sm A phase. The experiment allows for the estimation of the coupling constant, $C_s > 3 \times 10^{-3}\ \mathrm{Jm}^{-2}$, and indicates that the system is in the strong surface coupling regime. Because of the experimental limitations, the critical thickness very near the Sm A phase could not be determined unambiguously, so the question of the existence of a Lifshitz point in such a system is still open.

## 4. Optics of Ferroelectric Liquid Crystals in Magnetic Fields

Many of the interesting and fundamental properties of ferroelectric liquid crystalline phases can be conveniently studied by different optical and electrooptical techniques such as quasielastic light scattering, optical response measurements, selective reflection, optical interferometric techniques, etc. The reason for using optical spectroscopic methods in the analysis of thermodynamical properties of ferroelectric liquid

crystals lies in the strong coupling of the director field $\mathbf{n}(\mathbf{r},t)$ to the dielectric tensor field $\underline{\epsilon}(\mathbf{r},t)$, as well as in the high sensitivity and local probing of optical methods. Understanding the optical properties of ferroelectric liquid crystals, which are by themselves very attractive and interesting problems, is thus necessary. Although almost everything which is related to the problem of light propagation in these birefringent and helicoidally modulated structures seems hardly solvable analytically,[22] we would like to present here some simple views and basic concepts, which surprisingly can explain most of the basic optical phenomena in ferroelectric liquid crystals.

In the ferroelectric Sm C* phase, each smectic layer can be considered as a weakly biaxial Sm C phase, which is described by the dielectric tensor $\underline{\epsilon}$ with the eigenvalues $\epsilon_1$, $\epsilon_2$ and $\epsilon_3$

$$\underline{\epsilon} = \begin{bmatrix} \epsilon_1 & 0 & 0 \\ 0 & \epsilon_2 & 0 \\ 0 & 0 & \epsilon_3 \end{bmatrix}. \tag{25}$$

By symmetry arguments, one of the axis of the eigenframe (1,2,3) (e.g. $1 \parallel y \parallel C_2$) must be parallel to the $C_2$ axis. The difference between $\epsilon_1$ and $\epsilon_2$ is usually small, so that each layer of the Sm C* phase can be sometimes considered as an optically uniaxial layer, with the optical axis tilted at a tilt angle $\theta$ with respect to the helical axis.

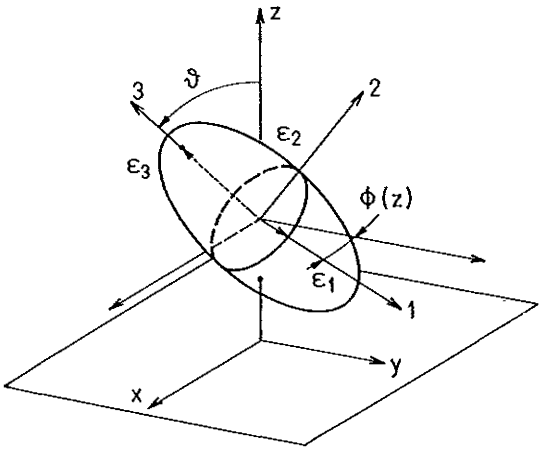


Fig. 9. Local orientation of the dielectric tensor in the Sm C* phase.

The dielectric tensor which defines the optical properties of the Sm C* phase is obtained by two successive rotations of the tensor $\underline{\epsilon}$, starting from the configuration where the eigenframe (1,2,3) coincides with the laboratory frame $(x,y,z)$, as shown in Fig. 9. First, the tensor $\underline{\epsilon}$ is rotated through the tilt angle $\theta$ around the $y$-axis followed by a rotation through the phase angle $\Phi(z)$ around the $z$-axis. The resulting

dielectric tensor can be written as a sum of three characteristic contributions

$$\underline{\epsilon} = \begin{bmatrix} \frac{1}{2}(\epsilon_1+\epsilon_2)+\frac{1}{2}(\epsilon_3-\epsilon_1)\sin^2\theta & 0 & 0 \\ 0 & \frac{1}{2}(\epsilon_1+\epsilon_2)+\frac{1}{2}(\epsilon_3-\epsilon_1)\sin^2\theta & 0 \\ 0 & 0 & \epsilon_1\sin^2\theta+\epsilon_3\cos^2\theta \end{bmatrix}$$

$$+ (\epsilon_3-\epsilon_1)\sin\theta\cos\theta \begin{bmatrix} 0 & 0 & \cos\Phi(z) \\ 0 & 0 & \sin\Phi(z) \\ \cos\Phi(z) & \sin\Phi(z) & 0 \end{bmatrix}$$

$$+ \frac{1}{2}\Big((\epsilon_1-\epsilon_2)+(\epsilon_3-\epsilon_1)\sin^2\theta\Big) \begin{bmatrix} \cos 2\Phi(z) & \sin 2\Phi(z) & 0 \\ \sin 2\Phi(z) & -\cos 2\Phi(z) & 0 \\ 0 & 0 & 0 \end{bmatrix}. \qquad (26)$$

The spatially inhomogeneous terms in the dielectric tensor of the Sm C* phase (i.e. the second and third terms) are typically a factor of $10^{-1}$ to $10^{-2}$ smaller than the principal values $\epsilon_i$. This suggests that for the optical properties of the Sm C* phase, a simple perturbative approach might be used, where spatially inhomogeneous terms of $\underline{\epsilon}(z)$ play the role of a small perturbation.

Following the approach of M. A. P. Peterson,[23] we define a tensor-weighted inner product of the two eigenfunctions $|\mathbf{k},p\rangle$ and $|\mathbf{k}',p\rangle$, characterized by the wave-vector $\mathbf{k}$ and the polarization $p$ as

$$\langle \mathbf{k}',p'|\mathbf{k},p\rangle = \langle \mathbf{E}_{\mathbf{k}',p'}|\mathbf{E}_{\mathbf{k},p}\rangle = \frac{1}{2\pi}\int d^3r\, \mathbf{E}_{\mathbf{k}',p'}\, \underline{\epsilon}(\mathbf{r})\, \mathbf{E}_{\mathbf{k},p}\,. \qquad (27)$$

Let $|\mathbf{k},p\rangle$ and $|\mathbf{k}',p'\rangle$ represent the eigensolutions of the wave equation in the inhomogeneous medium characterized by the dielectric tensor $\epsilon(\mathbf{r}) = \underline{\epsilon}_0 + \delta\underline{\epsilon}(\mathbf{r})$.

$$\Big\{\underline{\epsilon}_0^{-1}\,\nabla\times\nabla\times - \omega^2\,\underline{\epsilon}_0^{-1}\,\delta\underline{\epsilon}\Big\}|\mathbf{k},p\rangle = \omega^2|\mathbf{k},p\rangle\,. \qquad (28)$$

Here, the speed of light in vacuum is set to $c_0 = 1$. The above form of the wave equation is similar to the Schrödinger equation, and $\underline{\epsilon}_0$ and $\delta\underline{\epsilon}$ are the homogeneous and inhomogeneous parts of the dielectric tensor $\underline{\epsilon}$. It can be shown that the operator $\hat{A} = \underline{\epsilon}^{-1}\,\nabla\times\nabla\times$ is Hermitian with respect to the tensor-weighted inner product (Eq. (27)), so that the eigenvectors $|\mathbf{k},p\rangle$ are orthogonal and the $\omega^2(\mathbf{k},p)$ always real.

In the case of $\delta\underline{\epsilon} = 0$ we obtain the eigenvalue $\omega_0(\mathbf{k},p)$, describing the dispersion relation for the propagation of linearly polarized $\sigma$ and $\pi$ plane waves in a birefringent, uniaxial medium, which are denoted by $|\mathbf{k},\sigma\rangle$ and $|\mathbf{k},\pi\rangle$, respectively. The presence of a small ***periodic perturbation*** in the wave equation (Eq. (28)) significantly alters the situation. In particular, one has to introduce the ***concept of a Brillouin zone***, whereas the eigensolutions should obtain the ***Bloch form***, reflecting the appearance of a ***periodic perturbation*** term $\delta\underline{\epsilon}(z)$. Moreover, on

the basis of general considerations, one can expect that the periodic perturbation would have the strongest influence at the points of degeneration

$$\omega_0(\mathbf{k},\sigma) = \omega_0(\mathbf{k},\pi)\,. \tag{29}$$

Basic features of the optical spectrum can be obtained by applying a simple perturbative approach to the wave Eq. (28). The perturbed eigenvalue $\omega^2(\mathbf{k},p)$ is given by

$$\omega^2(\mathbf{k},p) = \omega_0^2(\mathbf{k},p)\left[1 - \frac{\langle \mathbf{k},p|\underline{\epsilon}^{-1}\delta\underline{\epsilon}|\mathbf{k},p\rangle}{\langle \mathbf{k},p|\mathbf{k},p\rangle} - \frac{1}{\langle \mathbf{k},p|\mathbf{k},p\rangle} \times \sum_{\mathbf{k}',p'} \frac{|\langle \mathbf{k},p|\underline{\epsilon}^{-1}\delta\underline{\epsilon}|\mathbf{k}',p'\rangle|^2}{(\omega_{\mathbf{k},p}^2 - \omega_{\mathbf{k}',p'}^2)\langle \mathbf{k}',p'|\mathbf{k}',p'\rangle}\right], \tag{30}$$

whereas the approximate solution is expressed in the form of a Bloch wave

$$|\mathbf{k},p\rangle = |\mathbf{k},p\rangle + \sum_{\mathbf{k}',p'} \frac{\omega_0^2(\mathbf{k},p)|\langle \mathbf{k}',p'|\delta\underline{\epsilon}|\mathbf{k},p\rangle|^2}{(\omega_0^2(\mathbf{k}',p') - \omega_0^2(\mathbf{k},p))\langle \mathbf{k},p|\mathbf{k},p\rangle}\,|\mathbf{k}',p'\rangle\,. \tag{31}$$

The above expressions show that the perturbation $\delta\underline{\epsilon}(z)$ plays the role of a periodic potential which couples the unperturbed eigenmodes $|\mathbf{k},\sigma\rangle$ and $|\mathbf{k},\pi\rangle$. Because $\delta\underline{\epsilon}$ contains two terms with spatial periods $q_c$ and $2q_c$, respectively, we can expect that the perturbation would mix unperturbed eigenwaves with wavevectors that differ by

$$\mathbf{k} - \mathbf{k}' = \mathbf{q}_c \quad \text{or} \quad 2\mathbf{q}_c\,, \tag{32}$$

where the corresponding unperturbed eigenvalues are degenerate, $\omega_0(\mathbf{k},\sigma) = \omega_0(\mathbf{k},\pi)$. In the ferroelectric liquid crystal this is fulfilled when light is propagating at a ***Bragg angle*** or ***along the helix.***

The most striking result of the presence of a periodic dielectric tensor $\delta\underline{\epsilon}(\mathbf{z})$ is the appearance of band gaps at the degeneration points, as shown in Fig. 10. This results in a ***band structure for the dispersion relation*** of the propagation of light in a weakly anisotropic, periodic medium, and strongly resembles the energy band structure for a particle, propagating in a periodic potential. One can see from Fig. 10 that a periodic perturbation induces frequency gaps in the originally degenerated points B and C. As a result, we obtain three characteristic reflection bands, which are centered at frequencies $\omega_B^+$, $\omega_C$ and $\omega_B^-$, respectively. Whereas the C-band is a total reflection band, where no light can propagate in the medium, the B-bands are selective reflection bands. Here, only a certain polarization of the incident light is reflected, whereas the light of the proper polarization can propagate in the liquid crystal. A similar band structure was obtained in a numerical analysis of the solutions of the wave equation in the Sm C* phase by Oldano.[24] The fact that this simple perturbative approach describes very well all the basic features of the optical spectrum of the Sm C* phase is a very nice illustration of the fact that

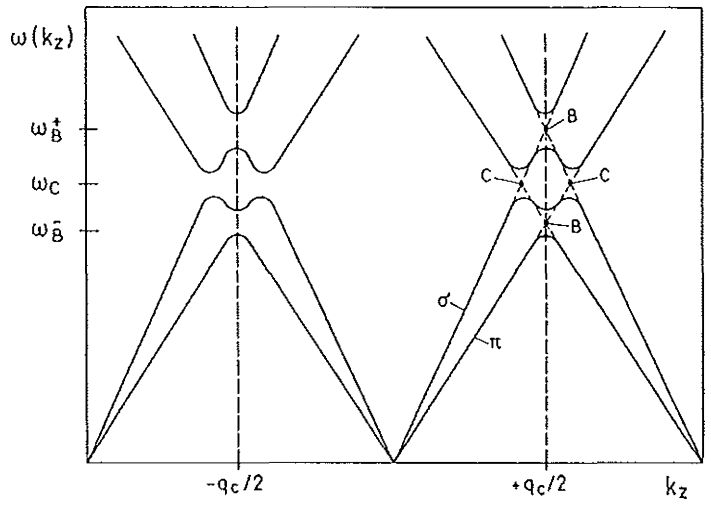


Fig. 10. The effect of a periodic perturbation $\delta\underline{\epsilon}(z)$ (see Eq. (26)) on the dispersion relation for light propagation in an optically uniaxial crystal. The figure is schematic, $k_z$ is the $z$-component of the wave-vector of light in the crystal, whereas $\sigma$ and $\pi$ denote the dispersion of the ordinary and extraordinary waves, respectively.

the origin of the basic optical phenomena in birefringent, modulated structures lies in the ***form and symmetry of the dielectric tensor*** and not in the magnitude of its components.

The first order approximation to the light propagation in a periodic, birefringent crystal is valid if the modulation of the dielectric tensor $\delta\underline{\epsilon}$ is small and the light does not propagate neither at the Bragg angle nor along the helical axis. The approximate solutions are just $\sigma$ and $\pi$ linearly polarized plane waves, whereas from Eq. (30) the first order corrected eigenvalue is

$$\omega^2(\mathbf{k},p) = \omega_0^2(\mathbf{k},p)\left(1 - \frac{\langle \mathbf{k},p|\underline{\epsilon}^{-1}\delta\underline{\epsilon}|\mathbf{k},p\rangle}{\langle \mathbf{k},p|\mathbf{k},p\rangle}\right). \tag{33}$$

Here, the second term in brackets is just the space averaged value of the inhomogeneous part of the dielectric tensor $\delta\underline{\epsilon}(z)$. Higher order corrections to the eigenvalue $\omega(\mathbf{k},p)$ include terms proportional to $|\langle \mathbf{k}',p'|\underline{\epsilon}_0^{-1}\,\delta\underline{\epsilon}|\mathbf{k},p\rangle|^2 \propto \theta^4$ and are important near the points of degeneration, i.e. near the edges of the Brillouin zone, introduced by the periodic form of the perturbation $\delta\underline{\epsilon}(\mathbf{r})$.

The first order corrected eigenvalue $\omega^2(\mathbf{k},p)$ in the presence of the perturbation $\delta\underline{\epsilon}(z)$ can be interpreted as a change in the refractive indices of the medium. This means that in this approximation the optical properties are described by the corresponding ***space-averaged uniaxial tensor*** $\langle\underline{\epsilon}\rangle$. The first order correction preserves the form of the normal wave surface, whereas the diagonal elements of

the corresponding space-averaged tensor $\langle\underline{\epsilon}\rangle$ are

$$\langle\underline{\epsilon}\rangle_{xx} = \frac{1}{2}(\epsilon_1+\epsilon_2)+\frac{1}{2}(\epsilon_3-\epsilon_1)\theta^2+\frac{1}{2}\Big((\epsilon_1-\epsilon_2)+(\epsilon_3-\epsilon_1)\theta^2\Big)\langle\cos 2\Phi(z)\rangle\,, \quad (34a)$$

$$\langle\underline{\epsilon}\rangle_{yy} = \frac{1}{2}(\epsilon_1+\epsilon_2)+\frac{1}{2}(\epsilon_3-\epsilon_1)\theta^2-\frac{1}{2}\Big((\epsilon_1-\epsilon_2)+(\epsilon_3-\epsilon_1)\theta^2\Big)\langle\cos 2\Phi(z)\rangle\,, \quad (34b)$$

$$\langle\underline{\epsilon}\rangle_{zz} = \epsilon_3-(\epsilon_3-\epsilon_1)\theta^2\,. \quad (34c)$$

In the undistorted helicoidal phase, where $\Phi(z)=\frac{2\pi}{p}z$, the spatial averages equal zero, i.e. $\langle\cos 2\Phi\rangle = 0$, and the dielectric tensor $\langle\underline{\epsilon}\rangle$ reduces to the uniaxial tensor with the optical axis parallel to the helical axis.

The components $\langle\underline{\epsilon}\rangle_{xx}$ and $\langle\underline{\epsilon}\rangle_{yy}$ depend on the magnitude of the external magnetic field $H$ through the space averaged values of $\langle\cos 2\Phi(z)\rangle = 1-2\langle\mathrm{sn}^2(u,k)\rangle$[25]

$$\langle\underline{\epsilon}(H)\rangle = \begin{bmatrix} \epsilon_x-\Delta(H) & 0 & 0 \\ 0 & \epsilon_x+\Delta(H) & 0 \\ 0 & 0 & \epsilon_{zz} \end{bmatrix}. \quad (35)$$

Here, $\epsilon_x = \frac{1}{2}(\epsilon_1+\epsilon_2)+\frac{1}{2}(\epsilon_3-\epsilon_1)\,\theta^2$ is the magnetic-field independent part, whereas the magnetic-field dependent part is

$$\Delta(H) = \frac{1}{2}\Big((\epsilon_1-\epsilon_2)+(\epsilon_3-\epsilon_1)\,\theta^2\Big)\left(2\frac{K(k)-E(k)}{k^2\,K(k)}-1\right). \quad (36)$$

In the limit of small fields, $H\to 0$, $\Delta(H)\to 0$, whereas near the critical field $H\to H_c$, $\Delta(H)\to\frac{1}{2}\Big((\epsilon_1-\epsilon_2)+(\epsilon_3-\epsilon_1)\,\theta^2\Big)$. As a consequence, in the zero-field limit, $\langle\underline{\epsilon}\rangle$ obtains the uniaxial form, whereas in the presence of a transverse magnetic field it obtains a biaxial form. This is an example of ***magnetic-field induced biaxiality*** in a distorted helicoidal phase. It should be stressed that the magnetic field induced biaxiality is here mainly the result of the global distortion of the phase of the order parameter and to a lesser extent the result of the intrinsic local biaxiality of the liquid crystal molecules.

The above model predicts a reduction of $\langle\underline{\epsilon}\rangle_{xx}$, whereas $\langle\underline{\epsilon}\rangle_{yy}$ is expected to increase with the increasing magnetic field. Although the overall changes of the components of $\langle\underline{\epsilon}\rangle$ are expected to be small, they should be observable at fields far below the critical field. In particular, magnetic field induced biaxiality in the ferroelectric phase with $\Delta\chi>0$ should be observable as a magnetic-field induced distortion of the conoscopic figure in a plane, perpendicular to the direction of the magnetic field, i.e. the $x$–$z$ plane. Figures 11a and 11b show the influence of an external magnetic field on the $x$–$z$ cross-sections of the normal wave surface of a ferroelectric liquid crystalline phase. In zero field, the section of a normal wave surface at $y=0$ consists of a circle and an oval, corresponding to the unperturbed ordinary ($\sigma$) and unperturbed extraordinary ($\pi$) wave, with the optical axis along $z$. The

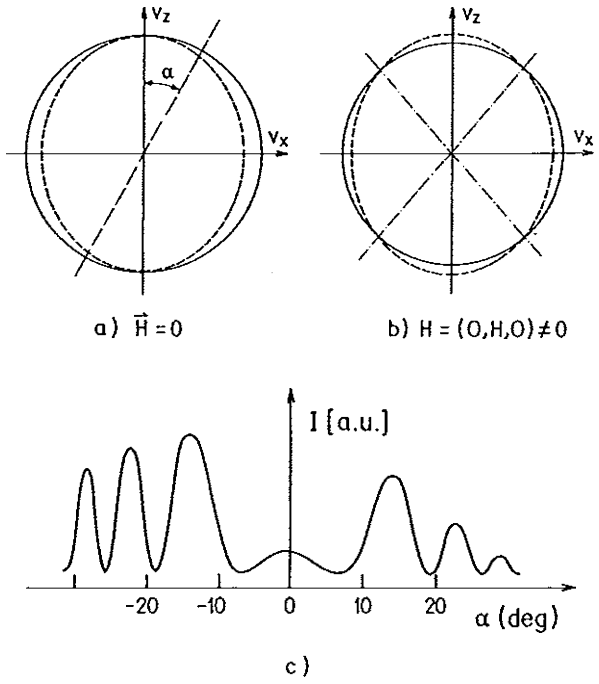


Fig. 11. The normal wave surface in the Sm C* phase for a) $H = 0$ and b) $H \neq 0$. The so-called conoscopic figure is shown in c) and results from the interference of the ordinary and extraordinary waves, propagating at an angle $\alpha$ with respect to the optical axis which is in the $z$-direction.

magnetic field dependence of the ordinary and extraordinary indices of refraction for the propagation of light in the $x$–$z$ plane are deduced from Eqs. (34) and (35):

$$n_0^2 = \langle \epsilon \rangle_{yy}(H) = \epsilon_x + \Delta(H)\,, \tag{37}$$

$$\frac{1}{n_e^2} = \frac{\sin^2\alpha}{\langle \epsilon \rangle_{zz}} + \frac{\cos^2\alpha}{\epsilon_x - \Delta(H)}\,. \tag{38}$$

Here, $\alpha$ is the angle between the direction of wave propagation and the $z$ axis. Under the influence of an external field, the circle, corresponding to the phase velocity of the ordinary wave $c = c_0/n_0$, contracts with increasing magnetic field, whereas the oval is deformed in the $z$-direction, as shown in Fig. 11b. The single optical axis at $H = 0$ splits into two optical axes, located symmetrically with respect to the $z$-axis. As a result of this splitting, the conoscopic figure which reflects the shape of the two normal wave surfaces is deformed in the $x$–$z$ plane. The deformation is most pronounced near the center of the conoscopic figure, where even a small change in the index of refraction induces a strong splitting between the two optical axes. Finally, very near the critical field, the angle $\beta$ between the two optical axis should saturate near the value $\tan(\beta/2) \approx \sqrt{\frac{\epsilon_3}{\epsilon_1}}\,\theta$.

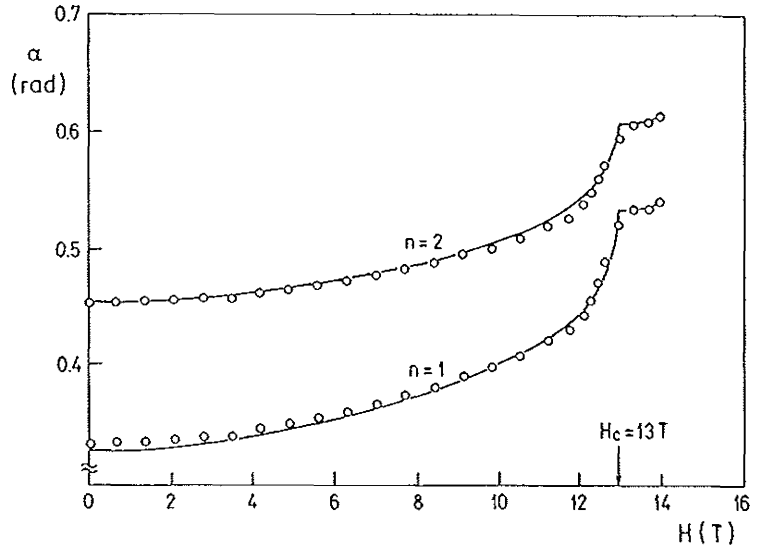


Fig. 12. Magnetic field induced shift of the position of the first ($n = 1$) and the second ($n = 2$) minima of the conoscopic figure in the antiferroelectric (AFE) phase of a liquid crystal MHPOBC.[25] The solid line represents the best fit within the first order approximation to the optics of chiral liquid crystals. The critical field for the unwinding of the AFE helical structure is 13 T and is observed as a point where the positions of the conoscopic minima saturate.

According to Eqs. (34) and (35), $\Delta(H)$ depends strongly on the magnitude of the tilt angle and the difference $\epsilon_3 - \epsilon_1$. This means that the deformation of the normal surfaces is very small near $T_c$, where the tilt angle is small and increases upon decreasing temperature. The influence of the magnetic field on the normal surface of a helicoidal smectic phase has recently[25] been observed in an interferometric study of the magnetic field induced distortion in an antiferroelectric liquid crystal and is shown in Fig. 12. An excellent agreement was found between the predicted and observed distortion of the normal surface.

## 5. Broken Symmetries and Gapless Phasons

One of the most striking features which can be observed near the Sm A→Sm C* phase transition is the ***spontaneous breaking*** of the point symmetry of the Sm A phase at the phase transition point $T_c$. The symmetry breaking is here the result of the spontaneous tilting of molecular directors in the Sm C* phase, which reduces the original $D_\infty$ point symmetry of the Sm A layers to the $C_2$ symmetry of the chiral Sm C* layers. The interesting aspect of this transition is the fact that the ***continuous point symmetry*** is broken. This has some very interesting and fundamental consequences for the order parameter dynamics and is in particular reflected in the spectrum of the so-called elementary excitations of the system. According to the Goldstone theorem,[26] as a result of the continuous symmetry

breaking a ***zero frequency symmetry restoring Goldstone mode*** appears in the Sm C* phase, which tries to restore the broken continuous symmetry of the Sm A phase.

The central idea of the conventional theory of spontaneous symmetry breaking at the phase transition point as first proposed by van Hove[27] and by Landau and Khalatnikov[28] is the ***critical slowing down*** of the order parameter excitations at $T_c$. This implies the existence of a mode $\omega_s(q,T)$ in the excitation spectrum $\omega(q,T)$, of which the relaxation rate goes to zero as we approach the phase transition from above

$$\omega^2(q,T) = \alpha(T - T_c) + k(q - q_c)^2\,, \quad T \geq T_c\,. \tag{39}$$

Thus for $T = T_c$ and $q = q_c$ the relaxation frequency of this mode equals zero

$$\omega_s(q_c, T_c) = 0\,. \tag{40}$$

This is the so-called ***soft mode*** of the transition in question. It is a symmetry breaking mode which freezes out at the phase transition point and breaks the symmetry of the higher temperature phase.

The concept of the soft mode was first introduced to the Sm A→Sm C* phase transition by Blinc and Žekš[29] in 1978. The theory was based on a simple nonequilibrium free-energy expansion (Eq. (3)) and analyzed the spectrum of the order parameter fluctuations within the Landau–Khalatnikov dynamical equations. Within this approach, the order parameter is expressed as a sum of a static and a time-fluctuating part, respectively,

$$\xi(z,t) = \xi_0(z) + \delta\xi(z,t)\,, \tag{41a}$$

$$\mathbf{P}(z,t) = \mathbf{P}_0(z) + \delta\mathbf{P}(z,t)\,. \tag{41b}$$

Here only the fluctuations $\delta\xi$ and $\delta\mathbf{P}$ with a wave vector along the $z$-axis are considered. After applying the Landau–Khalatnikov dynamical equations of motion, the spectrum of the elementary order parameter excitations can be divided into two groups of dispersion branches: the high frequency ***polarization modes***[30] and the low frequency ***director modes***. Whereas the polarization modes represent out-of phase fluctuations of $\delta\xi$ and $\delta\mathbf{P}$, the director modes represent the in-phase motion of $\delta\xi$ and $\delta\mathbf{P}$. The relaxation rates of polarization modes are typically in the 100 MHz region and are much faster than the relaxation rates of the director modes which are in the range of 1 Hz to 1 MHz. In the following we shall consider the dynamics of the director modes, which show critical behavior.

In the Sm A phase, the dynamical analysis of the nonequilibrium $g(z,t)$ (Eqs. (6) and (41)) gives a doubly degenerate ***soft-mode branch*** of excitations with a dispersion relation

$$\tau_S^{-1}(q) = \frac{\alpha}{\gamma}(T - T_c) + \frac{K_3}{\gamma}(q_c \pm q)^2\,. \tag{42}$$

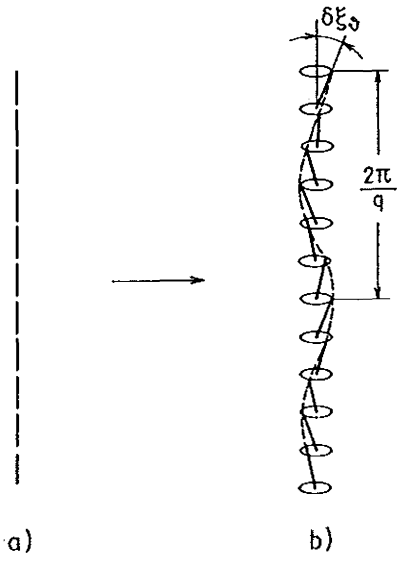


Fig. 13. Soft mode excitations in the Sm A phase of a chiral ferroelectric liquid crystal. The homogeneous equilibrium director field shown in a) is excited by the helical fluctuation as shown in b).

The soft mode dispersion branch is thus strongly temperature dependent and has a minimum at the wave vector $q_c$, which is the wave vector of the modulation of the Sm C* phase. In the Sm A phase the order parameter excitations have a form of helicoidally polarized overdamped plane waves with the wave vector $q$ (see Fig. 13)

$$\delta\xi_q(z,t) = \delta\xi_\theta \begin{bmatrix} \sin qz \\ \cos qz \end{bmatrix} e^{-t/\tau} . \tag{43}$$

As one can see, these excitations represent the helicoidal-like fluctuations of the tilt angle. Once the excitation is created by thermal excitation, it relaxes to zero in a characteristic relaxation time $\tau(q)$. The relaxation time for an excitation with a wave vector $q_c$ diverges as we approach the phase transition temperature $T_c$ from above

$$T \to T_c^+ : \quad \tau(q_c) \to \infty . \tag{44}$$

At the phase transition the soft mode excitation thus freezes-out in a form of a space coherent helical wave and creates a static helicoidal Sm C* structure.

By performing a similar dynamical analysis one obtains in the Sm C* phase two low-frequency dispersion branches, which originate from the soft mode branch at $T_c$. The so-called ***amplitudon dispersion branch*** represents the plane-wave-like excitations of the magnitude of the tilt angle. It is strongly temperature dependent and shows a parabolic dispersion of the form

$$\tau_A^{-1}(q) = \frac{2\alpha}{\gamma}(T - T_c) + \frac{K_3}{\gamma}(q_c \pm q)^2 . \tag{45}$$

The second branch which originates from the soft mode branch is the so-called ***phason dispersion branch*** and is here of particular interest because it is closely related to the symmetry breaking in the system. In the unperturbed Sm C* phase the phason modes represent the phase-wave-like fluctuations of the ***phase*** $\Phi(z,t)$ of the order parameter with a ***gapless dispersion relation*** at all temperatures below $T_c$

$$\tau_{Ph}^{-1}(q) = \frac{K_3}{\gamma}(q_c \pm q)^2 . \tag{46}$$

The phason mode with the wave vector $q = \pm q_c$ represents small ***rotations or, what is the same, a sliding of the helix as a whole*** along the helical axis, restoring the axial $D_\infty$ symmetry of the Sm A phase. It is the characteristic ***zero frequency symmetry restoring Goldstone mode*** of the transition and is a direct consequence of the spontaneous breaking of the continuous symmetry group $D_\infty$. The order parameter dynamics in the ferroelectric Sm C* phases can be studied by various spectroscopic methods. Because the fluctuations of the director field are strongly coupled to the fluctuations of the polarization field $\mathbf{P}(\mathbf{r},t)$ and to the fluctuations of the optical axis, dielectric spectroscopy and quasielastic light scattering spectroscopy are two methods which are most widely used here. Whereas dielectric spectroscopy measures the linear response of the system to a small perturbating electric field, quasielastic light scattering spectroscopy analyzes the time-correlation in the thermal noise of the system in question. Furthermore, in the dielectric spectroscopy one obtains information on the ***polar*** modes with wave vector $q = 0$, which can only couple to the homogeneous measuring electric field. In this respect, light scattering spectroscopy is far more advantageous because it allows the study of the dynamics of polar or nonpolar modes with wave vectors in the range of the wave-length of light which is used in the experiment. One can thus directly determine the ***dispersion relations*** for the order parameter excitations. This is of special importance when studying the phase transition into the inhomogeneous phase, where the soft mode condenses in a general point $q \neq 0$ of the reciprocal lattice.

The first indication of the soft-mode behavior in the vicinity of the Sm A→Sm C* phase transition was given by the linear electrooptic response experiment performed by S. Garoff and R. B. Meyer in 1977.[31] In their experiment, Garoff and Meyer measured the temperature dependence of the low-frequency susceptibility $\chi(q = 0\,,\, \omega \to 0)$ in the Sm A phase of ferroelectric liquid crystal DOBAMBC. The observed real part of the susceptibility clearly followed the Curie law at $T > T_c$

$$\chi'(q = 0\,,\, \omega \to 0) \propto \frac{1}{T - T_c + (K_3\, q_c^2/\alpha)}\ ,\ T > T_c \tag{47}$$

and saturated very near the transition temperature $T_c$. This is consistent with the expected behavior of a system, where the soft mode condenses at a nonzero wave vector, i.e. whenever we have a second order phase transition into an ordered and spatially inhomogeneous system.

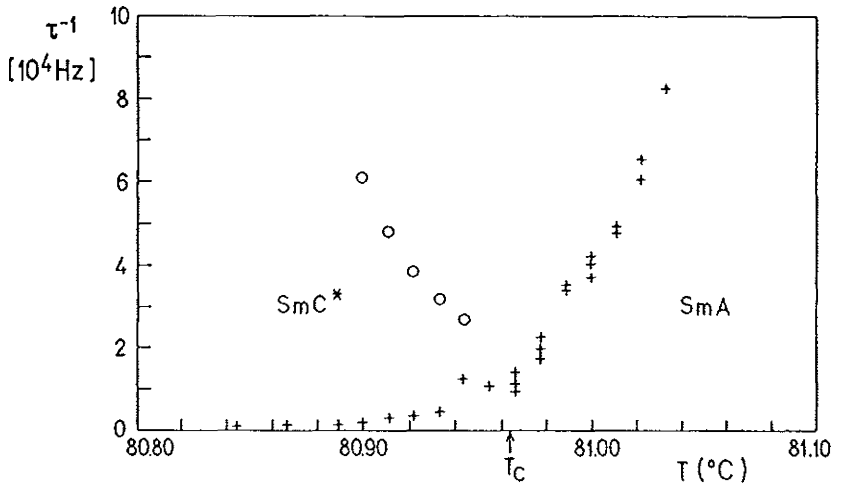


Fig. 14. Splitting of the soft mode into the amplitudon and phason modes near the Sm A→Sm C* transition in a ferroelectric liquid crystal 4-(2'-methylbutyl)phenyl 4'-n-octylbiphenyl-4-carboxylate (CE-8), see I. Drevenšek *et al.*[33] The scattering wave vector is noncritical, $\mathbf{q}_s \neq \mathbf{q}_c$, which results in finite relaxation rates at $T_c$.

The dynamical properties of ferroelectric liquid crystals in the vicinity of the Sm A→Sm C* phase transition became a subject of renewed interest in the late 80's. A series of dielectric dispersion[32] and light scattering experiments[33] were performed at that time which clarified the nature of the order parameter excitations near the Sm A → Sm C* phase transition. In particular, in the quasielastic light scattering experiments[33] a splitting of the soft mode branch into the amplitudon and phason dispersion branches was observed, as shown in Fig. 14. Moreover, it was observed that the soft mode dispersion branch is centered at $q \neq 0$ for $T > T_c$.[33] This is an indication that the soft mode freezes off-center in the reciprocal space.

Quasielastic light scattering experiments performed in the Sm C* phase revealed for the first time[33] the existence of a gapless phason dispersion branch, which is expected whenever the continuous symmetry group is broken at the phase transition point. The phason dispersion, as observed in DOBAMBC,[33] is shown in Fig. 15. One can see that the dispersion is centered at $q \neq 0$, which is characteristic of inhomogeneous systems. In the center of the dispersion, the observed phason relaxation rates are indeed very low, i.e. of the order of 10 Hz. The Goldstone mode, which is a phason mode with the wave vector in the center of the dispersion, is really a nearly zero-frequency mode. Recently, the study of the phason modes in modulated smectic phases has been extended to the recently discovered antiferroelectric Sm $C_A^*$[34] and ferrielectric Sm $C_\gamma^*$ phases.[35] Whereas the existence of a gapless Goldstone excitation was confirmed by the quasielectric light scattering experiments in the antiferroelectric phase[34] (see the inset to Fig. 15), its existence in ferrielectric phases is still controversial.

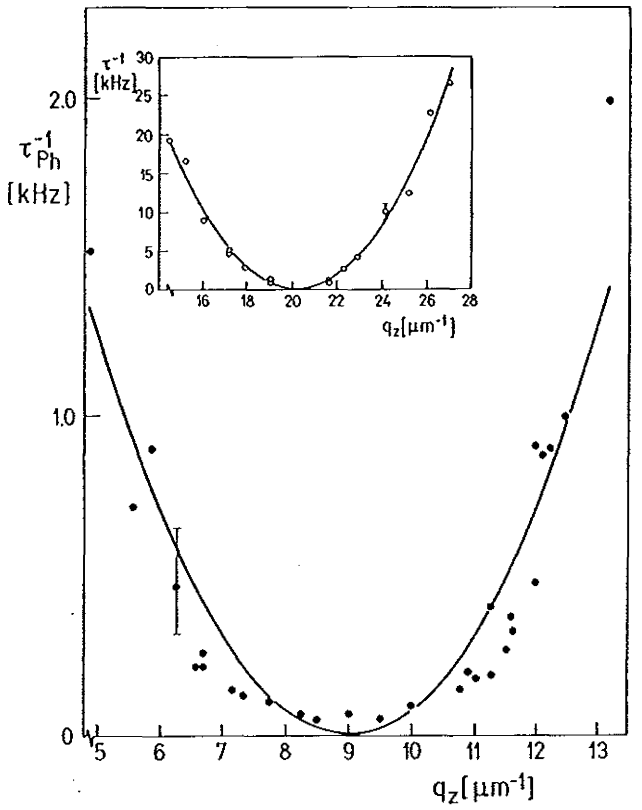


Fig. 15. Phason dispersion in the ferroelectric liquid crystal DOBAMBC.[33] The inset shows the phason dispersion in the antiferroelectric phase of the liquid crystal MHPOBC.[34]

The observed structure and temperature dependence of the spectrum of the order parameter excitations in the vicinity of the Sm A→Sm C* phase transition in the unperturbed ferroelectric liquid crystal are in general agreement with the predictions of a Landau theory. Here, the generalized Landau model does not qualitatively alter the structure of the order parameter excitation spectrum but merely introduces a temperature dependence, which reflects the temperature dependence of the period of the helix of the ferroelectric structure.

## 6. Symmetry Breaking by External Fields

When an external magnetic field is applied perpendicular to the helical axis of a ferroelectric liquid crystal, it distorts the helical arrangement of liquid crystalline molecules and induces a so-called soliton-like structure, for fields lower than the critical field $H_c$. This distortion of helical structure ***breaks the continuous helical symmetry*** of the unperturbed Sm C* phase, as can be easily seen by considering the symmetry properties of the unperturbed and distorted Sm C* phases. In the

unperturbed Sm C* phase any infinitesimal translation of the structure along the $z$-axis can be combined with a suitable infinitesimal rotation around the $z$-axis to transform the system into itself. The unperturbed Sm C* phase has thus a characteristic ***continuous helical symmetry***. On the contrary, the distorted Sm C* phase is invariant under a group of ***discrete transformations***, i.e. it is transformed into itself by a translation over half a period $p_0$ along the $z$-axis, followed by a 180° rotation around the helical axis.

This symmetry breaking by external fields has some deep and fundamental consequences for the spectrum of the order parameter excitations in ferroelectric liquid crystals. Here we shall discuss the magnetic-field effects on the phason excitation spectrum only, although similar phenomena can be expected for the behavior of the soft and amplitudon excitations as well. Many interesting consequences of the symmetry breaking by external fields can be understood by simply using symmetry arguments and analogies to other systems. For example, in the unperturbed Sm C* phase, the phason excitations which propagate along the helical axis exhibit a plane-wave behavior with a gapless and parabolic dispersion relation. Phason excitations are here just twist-bend-like elastic distortion waves, superposed onto the helical structure. When such an excitation propagates along the helix, it "sees" a smooth and uniformly twisted structure. All points of the helix are thus equivalent with respect to such an excitation, which results in the plane-wave nature of phason propagation in the unperturbed helix. However, when such a phason propagates in a magnetic-field distorted structure, it "sees" a regular and periodic array of $\pi$-soliton walls, resulting from the magnetic field induced breaking of the helical symmetry. This soliton-wall lattice, in combination with the coupling of the excitation to the external magnetic field, thus results in a ***periodic perturbation***, experienced by the phason as it propagates along the distorted helix.

The dynamics of a phason excitation in a soliton-like distorted Sm C* phase is thus analogous to the motion of a particle in an external periodic potential, which is a well-known and well understood problem. As a result of the presence of the periodic potential, the ***concept of a Brillouin zone*** (BZ) has to be introduced, whereas the excitation eigenfunctions obtain the ***Bloch form***. Perhaps the most striking consequence of the symmetry breaking by the external fields is the ***appearence of band gaps $G(q)$*** in the excitation spectrum $\omega(\mathrm{q},p)$, which becomes a periodic function in the reciprocal space, as shown schematically in Fig. 16.

The influence of an external magnetic field on the phason dispersion relation can be analytically calculated in the constant amplitude approximatio, thus neglecting the amplitudon contribution to the nonequilibrium free energy expansion. By writing the order parameter $\xi(z,t)$

$$\xi_x(z,t) = \theta \cos \Phi(z,t), \quad \xi_y(z,t) = \theta \sin \Phi(z,t), \tag{48}$$

where $\theta$ is the equilibrium tilt angle and $\Phi(z,t)$ is the phase of the order parameter, the phase-dependent part of the free-energy density $g(z,t)$ of the Sm C* phase in

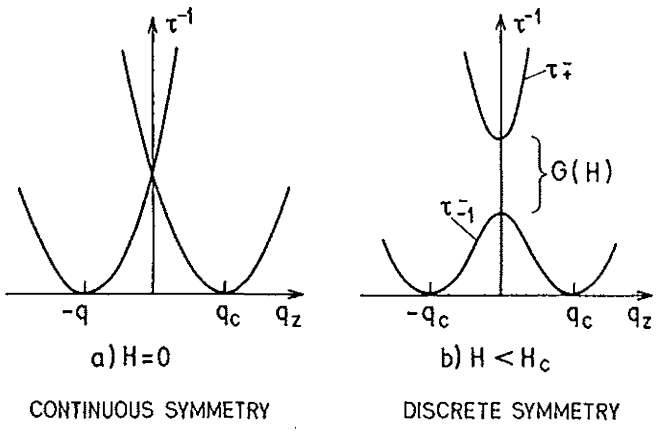


Fig. 16. Crossover from the continuous to the band structure of the phason dispersion relation, as a result of a symmetry breaking by an external magnetic field. The figure is schematic.

an external magnetic field $\mathbf{H} = (0, H, 0)$ is

$$g(z,t) = -\Lambda\theta^2 \frac{\partial\Phi(z,t)}{\partial z} + \frac{1}{2} K_3\theta^2 \left(\frac{\partial\Phi(z,t)}{\partial z}\right)^2 - \frac{1}{2}\Delta\chi H^2\theta^2 \sin^2\Phi(z,t). \quad (49)$$

The dynamics of small phase fluctuations $\delta\Phi(z,t)$ around the equilibrium phase $\Phi_0(z)$ (see Eq. (13))

$$\Phi(z,t) = \Phi_0(z) + \delta\Phi(z,t) \quad (50)$$

is analyzed within the framework of Landau–Khalatnikov dynamical equations. This leads to the overdamped form of the phason excitations (see also Eq. (38))

$$\delta\Phi(z,t) = \Psi(z)\, e^{-t/\tau}, \quad (51)$$

where $\tau = \tau(H)$ is the relaxation rate of the phason. The form of the eigenfunction $\Psi(z)$ is governed by the Lamé's equation of order one[36]

$$\frac{d^2\Psi}{du^2} + \left[h - 2k^2 \operatorname{sn}^2(u,k)\right]\Psi = 0. \quad (52)$$

Here, $h = k^2[\xi^2\gamma/(\tau(H)K_3 + 1]$ is the eigenvalue, $\gamma$ is the rotational viscosity, $\xi = \sqrt{K_3/(\Delta\chi H^2)}$ is the coherence length and $\operatorname{sn}(u,k)$ is the Jacobian sine amplitude with the argument $u = z/(\xi k)$ and modulus $k$, which is determined by the magnitude of the magnetic field, see Eq. (15).

The Lamé's equation of order one is exactly equivalent to the Schrödinger equation describing the propagation of a particle in a periodic soliton-like potential

$$V(u) = -2k^2 \operatorname{sn}^2(u,k). \quad (53)$$

The magnitude of this periodic potential is equal to $-2k^2$ and is in the limit of small field proportional to $H^2$. Thus for $H = 0$, $V(u) = 0$ and we are in the plane-wave regime. For $H \neq 0$ the periodic potential induces a band like structure of the phason spectrum with band gaps at the edges of the Brillouin zone. As is well-known, in the limit of small perturbation, the magnitude of the resulting gap $G(H)$ is proportional to the amplitude of the corresponding Fourier component $V_K$ of the periodic potential. In our case this is proportional to the square of the magnetic field, $G(H) \propto H^2$. Detailed analysis of the spectrum of the eigensolutions and eigenvalues of the Lamé's equation shows that the eigensolutions $\Phi(u)$ are given in a form of Bloch waves and can be calculated analytically.[37] The wave vector $q$ is ascribed to the particular eigensolution

$$\Psi(u) \rightarrow \Psi_q(u) \tag{54}$$

on the basis of the translational symmetry of this eigensolution.[37] Moreover, since the eigenvalues $h$ of the Lamé's equation determine the relaxation rate $\tau^{-1}(H)$ of the particular eigensolution $\Psi_q$, the dispersion relation $\tau^{-1}(q, H)$ for phasons propagating in a soliton-like lattice can be calculated analytically. This shows a surprising result, because ***only one forbidden gap*** $G(H)$ appears in the phason spectrum, separating the so-called ***optic-like*** branch from the ***acoustic-like*** excitation branch. This is in sharp contrast to the usually large number of forbidden gaps, which appear for example in the band theory of solids. The reason for this surprising result is the form of the periodic potential term $V(u) \propto -\mathrm{sn}^2(u, k)$, which was discussed in early work of Landau[38] and later by B. Sutherland[39] and by R. A. Cowley and A. D. Bruce.[40] This potential is peculiar in the sense that it exhibits a single bound state and a semicontinuum of free states, separated by a single gap.

The width of the Brillouin zone is determined by the period of the potential term $V(u)$ which is $p(H)/2$ and is field-dependent. This means that the reciprocal lattice vector equals to $|\mathrm{K}| = \frac{2\pi}{p(H)/2} = \frac{4\pi}{p(H)}$ and the corresponding Brillouin zone is $(-\frac{|\mathrm{K}|}{2}, +\frac{|\mathrm{K}|}{2}) \equiv (-q_c, +q_c)$. It should be stressed that the phason excitation, as introduced by Eq. (22), implies the use of a helical reference frame. As a consequence, the excitation with a wave vector $q$ in a helical reference frame is observable as an excitation with a wave vector $q \pm q_c$ in the laboratory frame. This has the consequence that the Brillouin zone is shifted by $\pm q_c$ and the zone boundaries and the band gap $G(H)$ are situated at $q = 0$ in the laboratory system.

The analysis of the eigenfunctions of the Lamé's equation shows that there are ***three distinct eigenfunctions*** with three distinct eigenvalues. At the edges of the Brillouin zone there are two ***real solutions*** which have the form of the Jacobian ***sine*** and ***cosine amplitudes***, respectively. Their relaxation rates show reverse field-behavior: whereas the relaxation rate of the first eigensolution increases with increasing field, the relaxation rate of the second eigensolution decreases with increasing field, as shown in Fig. 17,

$$\Psi_1(u) = \mathrm{sn}(u, k) \; : \qquad \tau_+^{-1}(H) = \frac{\Delta\chi}{\gamma} \frac{1}{k^2} H^2, \tag{55a}$$

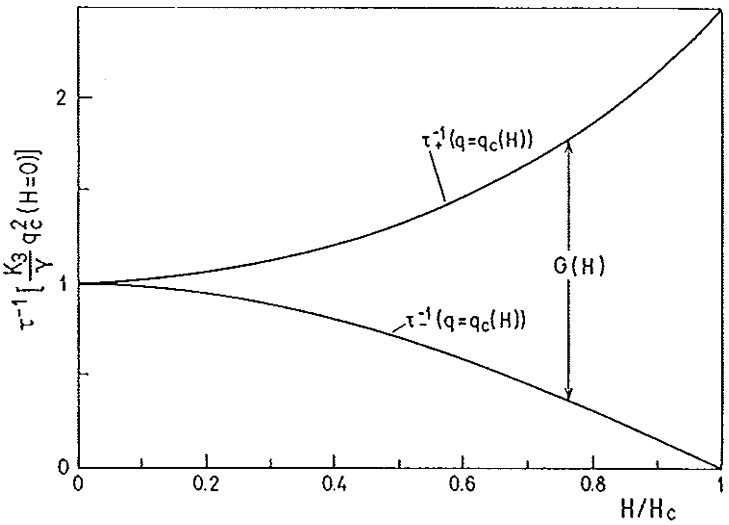


Fig. 17. Magnetic field dependencies of the relaxation rates of the optic-like $\tau_+^{-1}$ and the acoustic-like phason $\tau^{-1}$ at the edges of the Brillouin zone, as calculated from the Eqs. (55a) and (55b).

$$\Psi_2(u) = \mathrm{cn}(u,k) \; : \qquad \tau_-^{-1}(H) = \frac{\Delta\chi}{\gamma}\,\frac{1-k^2}{k^2}\,H^2 \,. \tag{55b}$$

The magnetic-field induced gap is thus proportional to the square of the applied field

$$G(H) = \tau_+^{-1}(H) - \tau_-^{-1}(H) = \frac{\Delta\chi}{\gamma}\,H^2 \,. \tag{56}$$

The third distinct eigensolution is obtained in the center of the Brillouin zone. It is given in a form of the Jacobian delta amplitude $\mathrm{dn}(u,k)$ and has a ***zero relaxation rate for all fields below*** $H_c$

$$\Psi_3(u) = \mathrm{dn}(u,k) \; : \qquad \tau^{-1}(H) = 0 \,. \tag{57}$$

It is interesting to see what is the physical interpretation of these eigenfunctions. The first one (Eq. (55a)) has the nodes in the center of the domain walls and represents the fluctuations of the shape of the domain walls. The eigensolution $\Psi_2(u)$ has the nodes in the middle of two neighboring domain walls and represents coherent, out-of-phase motion of the domain walls. The third eigensolution, $\Phi_3(u)$, is the Goldstone mode and represents the sliding of the helix as a whole along the $z$-direction. It is interesting to note that in the presence of the field the sliding of the helix is not any more equivalent to a rotation of the helix, as we have noted in the discussion of the gapless phason in an unperturbed helix. It is also very indicative that the Goldstone mode, which is a zero frequency symmetry restoring mode, exists in the distorted Sm C* phase as well.

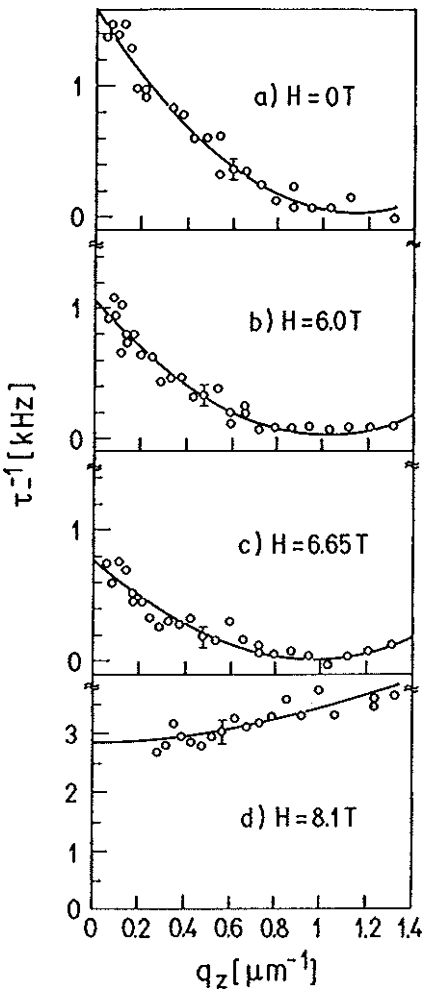


Fig. 18. The dispersion of the acoustic-like phason branch as determined in the Sm C* phase of a 35%:65% mixture of a chiral and racemic 4-(2'-methylbutyl)phenyl 4'-n-octylbiphenyl-4-carboxylate (CE-8) for different magnetic fields at $T_c - T = 3$ K. The critical field is 8 T and the solid lines are the best parabolic fits.[36,37]

The first observation of the magnetic-field induced splitting of the phason excitation was reported in a quasielastic light scattering experiment in high magnetic fields.[36] The observed dispersions of the acoustic phason branch in a mixture of chiral and racemic 4-(2'-methylbutyl)phenyl 4'-n-octylbiphenyl-4-carboxylate (CE-8) at $H = 0$, $H = 6.0$ T, $H = 6.65$ T and $H = 8.1$ T are shown in Figs. 18a, b, c and d, respectively. The critical magnetic field in this material was approximately 8 T, and depended slightly on the sample used in the experiment. One can observe the decrease of the phason relaxation rates at small wave vectors, which is characteristic of the acoustic-like phason modes at the edge of the BZ. At the same time, the

dispersion is slightly shifted towards smaller wave vectors, indicating the shrinking of the BZ. Slightly above the critical field, see Fig. 18d, the dispersion is centered at $q = 0$ and shifted to higher frequencies. This indicates a phase transition from the modulated phase, where the center of the dispersion is at a finite wave vector, into the homogeneous phase, where the dispersion is centered at $q = 0$. The magnetic field dependence of the optic-like phason modes at the edge of the BZ could not be determined by the quasielastic light scattering because of the small scattering intensity from the modes. Therefore dielectric spectroscopy was used in the experimental geometry, where only the optic-like phason modes at the edge of the zone contribute to the response of the system. The resulting magnetic-field dependencies of the phason relaxation rates together with a fit to the theoretical predictions are shown in Fig. 19 and clearly show the magnetic field induced splitting of the phason spectrum. The resulting gap $G(H)$ is shown in Fig. 20 up to the highest available field of 14 T and shows an excellent agreement with theoretical predictions.

A particularly interesting issue of the observed magnetic-field dependencies of the phason relaxation rates is the disappearance of the zero-frequency Goldstone mode beyond the critical magnetic field $H_c$. It turns out that this has a very fundamental origin in the spontaneous breaking of the point symmetry of the Sm A phase. At zero field, both the continuous rotational symmetry group $D_\infty$ as well as the continuous translation symmetry of the Sm A phase is broken, which is the reason for the existence of a zero-frequency symmetry restoring Goldstone mode. For fields ***below the Lifshitz field***, the Sm A→Sm C* phase transition is accompanied by the breaking of the discrete symmetry $D_2$ into $C_2$, but at the

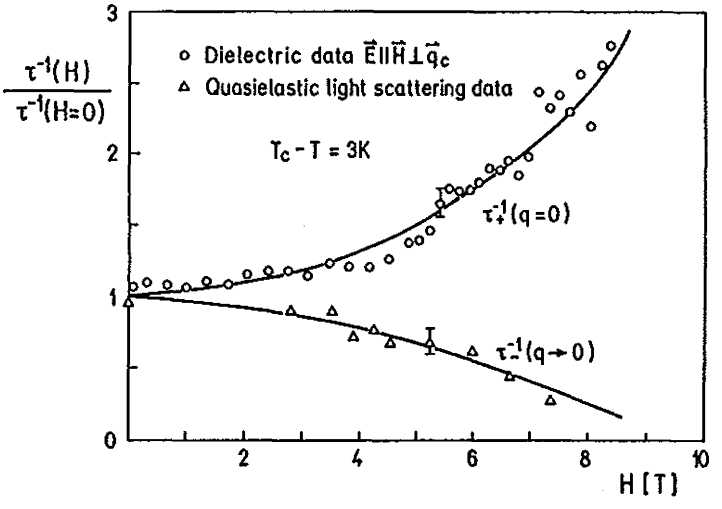


Fig. 19. Magnetic-field dependencies of the normalized relaxation rates of the acoustic-like and the optic-like phason modes in the Sm C* phase of a 35%:65% mixture of a chiral and racemic 4-(2'-methylbutyl)phenyl 4'-n-octylbiphenyl-4-carboxylate (CE-8) at $T_c - T = 3$ K and $q = 0$. The solid lines are the best fits to Eqs. (55a) and (55b), respectively.[36,37]

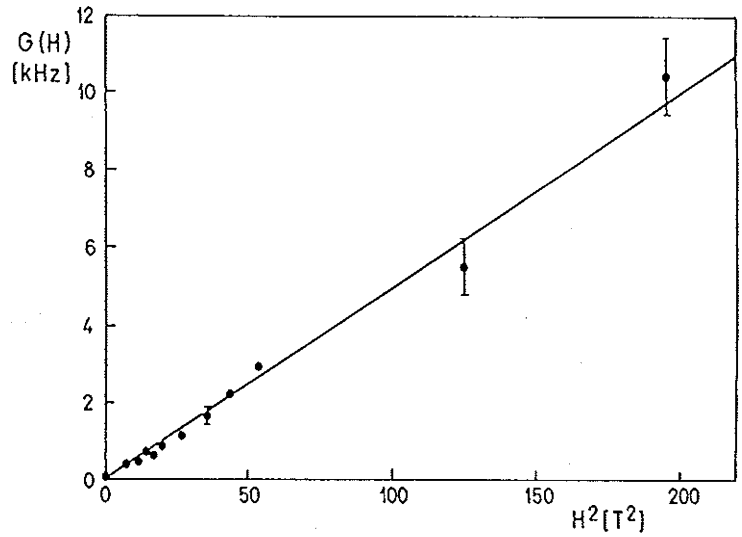


Fig. 20. Magnetic field dependence of the phason band gap in the Sm C* phase of a 35%:65% mixture of a chiral and racemic 4-(2'-methylbutyl)phenyl 4'-n-octylbiphenyl-4-carboxylate (CE-8) at $T_c - T = 3$ K and $q = 0$. The solid line is the best fit to the Eq. (56).[36,37]

same time the continuous translation symmetry of the Sm A phase is broken into the ***discrete translation symmetry*** of the soliton-like distorted Sm C* phase. Thus, the Goldstone mode is still expected to exist and it should appear in a form of a sliding translational wave, which tries to restore the broken translational symmetry of the Sm A phase. Finally, beyond the Lifshitz field $H_L$ only a discrete point symmetry is broken at the Sm A→Sm C phase transition and a zero frequency mode should not exist.

Let us conclude the discussion of symmetry breaking and collective excitations with some remarks on the effects of external electric fields. For high frequency AC fields, which couple to the dielectric anisotropy tensor quadratically, the effect on the spectrum of collective excitations is expected to be exactly equivalent to the magnetic field effects. In this case, the splitting of the phason spectrum appears at $q = 0$ and should thus be observable, for example, with the dielectric spectroscopy in two different experimental geometries, as shown in Sec. 7. The effect of a DC field, which couples linearly to the polarization, is quite different. First, instead of a $\pi$-soliton lattice we have here a $2\pi$-soliton lattice. As a result, the period of the perturbation for phason propagation which has its origin in the formation of soliton walls is equal to the period $p(E)$ of the helix in the case of an applied electric field. This is quite different from the magnetic field, where the period of the perturbation is equal to $p(H)/2$. As a result, the size of the Brillouin zone is two times smaller in the case of a DC electric field than in the case of a magnetic field. Following a simple construction of the Brillouin zone, we see that in an external DC electric field the band gaps appear outside the center of the reciprocal lattice, i.e. at the

wave vector $q_c/2$. Consequently, ***the phason splitting cannot be observed with dielectric spectroscopy in a DC field***, but can be observed in a quasielectric light scattering experiment. For a more detailed elaboration of this problem see Ref. 37.

## 7. Quasielastic Light Scattering and Optically Detected Dielectric Spectroscopy

In the ferroelectric Sm C* liquid crystal, collective excitations of the order parameter $\xi(\mathbf{r},t)$ are strongly coupled to the dielectric tensor field $\underline{\varepsilon}(\mathbf{r},t)$ and the spontaneous polarization field $\mathbf{P}(\mathbf{r},t)$. In an experiment they are thus observable as collective, spatially correlated reorientations of the optical axis or the dipole moment, respectively. The relaxation rates of the order parameter excitations are in the range from 10 Hz to 1 MHz, and can relatively easily be observed in quasielastic light scattering experiments and in dielectric spectroscopy. Whereas the quasielastic light scattering allows for the determination of the dispersion relations $\tau^{-1}(\mathbf{q})$ for the order parameter excitations, dielectric spectroscopy measures the response of the system at the wave vector $\mathbf{q} = 0$.

Quasielastic light scattering, or Rayleigh scattering spectroscopy, is a well-known optical spectroscopic method, which is very useful for the study of elementary excitations in liquid crystals. Because of extremely large optical birefringencies and very low relaxation rates, the orientational fluctuations in liquid crystals scatter light strongly. Light scattering in liquid crystals can be as high as a million time stronger than in optically isotropic liquids. In the quasielastic light scattering experiment one measures the time correlation of the intensity of scattered light at different scattering wave vectors. This allows the determination of the thermally excited dynamics of the system under study. The quasielastic light scattering in liquid crystals thus plays a similar role as the inelastic neutron scattering in the study of phonon excitations in solid crystals. The magnitude of the scattering wave vectors which are accessible in a light scattering experiment depends on the scattering geometry and the wavelength of the laser light. We can thus probe the most interesting interval in the reciprocal space (i.e. the first BZ of the Sm C* phase) by a proper selection of the scattering geometry. The magnitude of the BZ can also be adjusted by mixing right- and left-handed enantiomers to 1–10 $\mu m^{-1}$, the inverse of which falls with the range of accessible laser sources.

There is, however, one important difference between neutron scattering in solids and light scattering in liquid crystals, which originates from the extremely high optical anisotropies of liquid crystals. Liquid crystalline phases are optically uniaxial or biaxial materials with exceptionally large birefringence of the order of $\Delta n \approx 0.1$–$0.2$. This birefringence is orders of magnitude larger than in other materials. In spatially homogeneous liquid crystalline phases such as N, Sm A and Sm C, light can propagate as an ordinary or an extraordinary linearly polarized wave. These waves are scattered from thermally excited fluctuations of the dielectric tensor and

the scattered light can again propagate as an ordinary or extraordinary wave. In liquid crystals, an ordinary wave can thus be scattered into an extraordinary (o–e scattering) or an ordinary wave (o–o scattering), respectively. The situation with the extraordinary wave is similar, so that light scattering in liquid crystals is strongly polarization dependent.

In the first order approximation, which is expected to be valid far from degeration points, the helicoidal Sm C* phase is treated as a slightly perturbed optically uniaxial crystal. The eigenwaves of light propagation are linearly polarized ordinary $|\mathbf{k}, \sigma\rangle$ and extraordinary $|\mathbf{k}', \pi\rangle$ waves, with the wave vectors k and k′ and polarizations $\sigma$ and $\pi$, respectively. Thermal excitations of the order parameter field $\boldsymbol{\xi}(\mathbf{r}, t)$ result in the fluctuations of the dielectric tensor field

$$\boldsymbol{\xi}(\mathbf{r}, t) = \boldsymbol{\xi}_0(\mathbf{r}) + \delta\boldsymbol{\xi}(\mathbf{r}, t) \quad \Rightarrow \quad \underline{\epsilon}(\mathbf{r}, t) = \underline{\bar{\epsilon}}(\mathbf{r}) + \delta\underline{\epsilon}(\mathbf{r}, t)\,. \tag{58}$$

Here, $\underline{\bar{\epsilon}}(\mathbf{r})$ denotes the time average tensor, whereas $\delta\boldsymbol{\xi}(z, t) = (\delta\xi_\theta(z, t),\ \delta\xi_\Phi(z, t))$ is the deviation of the order parameter from the equilibrium, which scatters light quasielastically. In a scattering process, the incident light with wave vector k and polarization $p$ is scattered from thermal fluctuation $\delta\underline{\bar{\epsilon}}(\mathbf{r}, t)$ into a light wave with wave vector k and polarization p′.

In the limit of small $\theta$, the fluctuating part of the dielectric tensor $\delta\underline{\epsilon}(z, t)$ is derived from Eq. (26) in terms of the nonequilibrium order parameter as

$$\begin{aligned}\delta\underline{\epsilon}(z, t) \propto (\epsilon_3 - \epsilon_1) &\begin{bmatrix} 0 & 0 & \cos\Phi_0(z) \\ 0 & 0 & \sin\Phi_0(z) \\ \cos\Phi_0(z) & \sin\Phi_0(z) & 0 \end{bmatrix} \delta\xi_\theta(z, t) \\ + (\epsilon_3 - \epsilon_1) &\begin{bmatrix} 0 & 0 & -\sin\Phi_0(z) \\ 0 & 0 & \cos\Phi_0(z) \\ -\sin\Phi_0(z) & \cos\Phi_0(z) & 0 \end{bmatrix} \delta\xi_\Phi(z, t)\,.\end{aligned} \tag{59}$$

Here, $\delta\xi_\theta$ and $\delta\xi_\Phi$ represent the amplitudon and the phason excitations respectively, and $\Phi_0(z)$ is the equilibrium phase profile. From the above expression we see that the excitations of the order parameter can indeed be observed as the excitations of the dielectric tensor field $\delta\underline{\epsilon}(z, t)$

$$\delta\epsilon_{xz}(z, t) \propto (\epsilon_3 - \epsilon_1)\left[\delta\xi_\theta \cos(q_c z) - \delta\xi_\Phi \sin(q_c z)\right] = (\epsilon_3 - \epsilon_1)\,\delta\xi_x(z, t)\,, \tag{60}$$

$$\delta\epsilon_{yz}(z, t) \propto (\epsilon_3 - \epsilon_1)\left[\delta\xi_\theta \sin(q_c z) + \delta\xi_\Phi \cos(q_c z)\right] = (\epsilon_3 - \epsilon_1)\,\delta\xi_y(z, t)\,. \tag{61}$$

The fluctuations of the off-diagonal terms are thus observable as a strong depolarized scattering between the ordinary and extraordinary waves or vice versa.

Following the standard approach[41] to the scattering of a monochromatic plane wave with polarization i, wave vector $\mathbf{k}_i$, frequency $\omega_i$ and amplitude $E_0$

$$E_i = \mathrm{i}\, E_0\, e^{i\mathbf{k}_i\mathbf{r} - i\omega_i t} \tag{62}$$

from the fluctuations of the dielectric tensor $\delta\underline{\epsilon}(\mathbf{r}, t)$, the projection of the scattered electric field amplitude $\mathbf{f} \cdot \mathbf{E}_s$ at a distance $\mathbf{R}$ from the sample is

$$E_s(\mathbf{R}, t) = \mathbf{f} \cdot \mathbf{E}_s(\mathbf{R}, t) = -\frac{|k_i|^2\, E_0}{4\pi\, R\epsilon_0}\, e^{i\mathbf{k}_f\mathbf{R} - i\omega_i t} \delta\epsilon_{if}(\mathbf{q}_s, t)\,. \tag{63}$$

Here, $\mathbf{q}_s$ is the scattering wave vector, $\mathbf{q}_s = \mathbf{k}_i - \mathbf{k}_f$, and

$$\delta\epsilon_{if}(\mathbf{q}, t) = \int d^3 r\, \{\mathbf{f} \cdot (\delta\underline{\epsilon}(z, t)) \cdot \mathrm{i}\}\, e^{i\mathbf{q}_s\mathbf{r}} \tag{64}$$

is the Fourier transform of the fluctuating part of the dielectric tensor, projected onto the polarizations i and f of the incoming and the scattered beam, respectively. In a light scattering experiment, the time autocorrelation function

$$G^{(2)}(\tau) = \langle I(0)\, I(\tau)\rangle = \lim_{T\to\infty} \frac{1}{T} \int_0^T dt\, I(t)\, I(t+\tau) \tag{65}$$

of the scattered light intensity $I(t)$ is detected. Usually, a small portion of a coherent, elastically scattered field $E_{\mathrm{LO}}$ is mixed with the quasielastically scattered field $E_s$, so that the experiment is in the so-called heterodyne regime. In this case, $G^{(2)}(\tau)$ is proportional to the autocorrelation function of the Fourier component of the dielectric tensor field

$$G^{(2)}(\tau) \simeq \mathrm{Re}\{\langle \delta\epsilon_{if}(\mathbf{q}_s, 0)\, \delta\epsilon^*_{if}(\mathbf{q}_s, \tau)\rangle\}\,. \tag{66}$$

In the case of scattering of ordinary polarized light, $\mathbf{i} = (0, 1, 0)$, into extraordinary polarized light, $\mathbf{f} = (\sin\alpha, 0, \cos\alpha)$, the projection $\delta\epsilon_{if}(z, t)$ is

$$\mathbf{f}\, \delta\underline{\epsilon}(z, t)\, \mathbf{i} \simeq (\epsilon_3 - \epsilon_1)\Big[\cos\Phi_0\, \delta\xi_\Phi(z, t) + \sin\Phi_0 \delta\xi_\theta(z, t)\Big] \simeq \delta\xi_y(z, t)\,. \tag{67}$$

The scattering amplitude in this geometry is thus proportional to the $\delta\xi_y$ component of the order parameter, which is in turn proportional to the phase and amplitude fluctuations (see Eq. (60)).

In the unperturbed Sm C* phase, $\Phi_0(z) = q_c z$, and the order parameter excitations $\delta\xi_i^0(z, t) = \delta\xi_i^0 \cos(qz + \phi_i)\, e^{-t/\tau}$ are plane waves with wave vector $q$. The Fourier component $\delta\epsilon_{if}(q_s, t)$ at the scattering wave vector $q_s$ is nonzero if the wave vector of the excitation equals

$$q = \pm q_s \pm q_c\,. \tag{68}$$

The corresponding autocorrelation function of the scattered light intensity $G^{(2)}(\tau, q_s)$ in the heterodyne regime then consists of two distinct, exponentially decaying contributions from the phason and the amplitudon excitations, respectively

$$G^{(2)}(\tau, q_s) \simeq \langle \delta\xi_\Phi(q,t)\,\delta\xi_\Phi(q,t+\tau)\rangle + \langle \delta\xi_\theta(q,t)\,\delta\xi_\theta(q,t+\tau)\rangle$$
$$= \langle (\delta\xi_\Phi^0(q,t))^2\rangle\, e^{-\tau/\tau_\Phi} + \langle (\delta\xi_\theta^0(q,t))^2\rangle\, e^{-\tau/\tau_\theta}\,. \tag{69}$$

Here, $\langle (\delta\xi_i^0(q,t))^2\rangle$ is the mean square amplitude of the phason and the amplitudon excitation, respectively. The quasielastic light scattering experiment should thus allow the determination of both relaxation rates. In practice, the situation is somewhat complicated in view of the large differences in the relaxation rates of the amplitude and phase modes which result in large differences in the corresponding scattering amplitudes. The amplitudon modes, which have much higher relaxation rates, have correspondingly smaller amplitudes and are more difficult to observe.

Similar analysis can be performed in the case of a distorted Sm C* phase. Here the equilibrium phase equals $\sin\Phi_0(z) = \mathrm{sn}(u,k)$ and the eigenfunctions $\delta\xi_i(z)$ have the form of Bloch waves. This results in a slightly modified condition for the nonzero Fourier component of $\delta\epsilon_{if}(q,t)$ for a given excitation

$$q = \pm q_s \pm m * q_c \quad ; \quad \text{for } m \text{ integer}\,. \tag{70}$$

Whereas the condition (Eq. (68)) for the observation of the order parameter excitations in the unperturbed Sm C* phase can be interpreted as the shift of the original BZ by the reciprocal vector $\pm q_c$, the above condition reflects the periodicity of the dispersion relation in the reciprocal lattice of a distorted Sm C* phase.

In contrast to the quasielastic light scattering spectroscopy which allows for the determination of the dispersion relation of the order parameter excitations, the dielectric spectroscopy is a very useful probe for determining the susceptibilities of the soft, amplitude and phase modes at $q = 0$. This method suffers an inherent deficiency of probing a rather thin book-shelf aligned sample with a large surface area. Such a restricted planar geometry can in principle induce such a band structure of phason excitations via the surface-induced deformation of the helical structure.

This problem can be circumvented by an optical detection of the linear response of the Sm C* phase to a small external field.[42] This technique can be used in book-shelf as well as homeotropically aligned smectic phases. A small in-plane external electric field $\mathbf{E}_0\, e^{i\omega t}$ is applied to the homeotropic aligned Sm C* phase. This field couples linearly to the spontaneous polarization P and induces a phase distortion $\delta\phi(z)$ with the amplitude

$$\delta\phi(z) = \phi_0 \sin(q_c z) = -\frac{|E_0 \parallel P_0|}{K_3\, q_c^2 \theta^2}\, \frac{1}{1 + i\frac{\omega\gamma}{K_3 q_c^2}}\, \sin(q_c z)\,. \tag{71}$$

The electric field thus couples to the phason mode at the edge of the Brillouin zone. Here, $P_0$ and $\theta$ are the magnitudes of the spontaneous polarization and the tilt

angle, respectively. The induced phase distortion $\delta\phi(z)$ is reflected in the distortion of the dielectric tensor for the optical frequencies used. In the limit of small tilt angle, thus neglecting terms of the order of $\theta^2$ in $\delta\underline{\epsilon}(r)$, the space periodic part of the dielectric tensor changes under the influence of the measuring electric field

$$\delta\underline{\epsilon}(z) \approx \begin{bmatrix} 0 & 0 & \cos(\Phi_0(z)+\delta\phi) \\ 0 & 0 & \sin(\Phi_0(z)+\delta\phi) \\ \cos(\Phi_0(z)+\delta\phi) & \sin(\Phi_0(z)+\delta\phi) & 0 \end{bmatrix} . \tag{72}$$

As we have shown, at small tilt angles, the first order approximation to be valid and the ***space averaged dielectric tensor*** $\langle\underline{\epsilon}(\mathbf{r})\rangle$ determines the optical properties of the Sm C* phase. After linearizing $\delta\underline{\epsilon}(z)$ in $\delta\phi(z)$, the space averaged dielectric tensor of the Sm C* phase, perturbed by a small electric field, is

$$\langle\underline{\epsilon}(\mathbf{r})\rangle = \begin{bmatrix} a & 0 & \delta \\ 0 & a & 0 \\ \delta & 0 & b \end{bmatrix} . \tag{73}$$

Here, $a = \epsilon_1 + \frac{1}{2}(\epsilon_3 - \epsilon_1)\sin^2\theta$, $b = \epsilon_1 + (\epsilon_3 - \epsilon_1)\cos^2\theta$ and

$$\delta = \frac{1}{2}\phi_0(\epsilon_3 - \epsilon_1)\sin\theta . \tag{74}$$

The influence of a small external field to the average dielectric tensor is shown in the $\delta$-term, which is field-dependent via $\phi_0(E)$. As a result of a small external field, nonzero, off-diagonal terms appear in the dielectric tensor. This form of the dielectric tensor can be obtained by rotating the originally diagonal dielectric tensor with the principal values $\epsilon_1 = \epsilon_2 = a$ and $\epsilon_3 = b$ around the $y$-axis, i.e. around the electric field direction. The phase distortion, as induced by the external field, thus ***results in a small rotation of the effective dielectric tensor***, which represents a small rotation of the optical axis around the direction of the external field. The angle of the rotation $\eta$ of the optical axis is in the limit of a small distortion proportional to the external field

$$\eta(E,\omega) = \frac{1}{2}\frac{|E_0 \parallel P_0|}{K_3\, q_c^2 \theta}\,\frac{1}{1 + i\frac{\omega\gamma}{K_3\, q_c^2}} \tag{75}$$

and can easily be detected by an optical interferometric technique. From the frequency dependence of the linear electrooptic response, one can determine the relaxation rate $\frac{K_3}{\gamma}\, q_c^2$ of the phason mode at the edge of the BZ of the Sm C* phase.

A similar analysis can also be applied to the linear response of a magnetic-field distorted helicoidal Sm C* phase, with some particular differences. First, the single mode at the edge of the BZ splits into an acoustic and optic-like mode, and second, in view of the periodicity of the phason dispersion relation, an infinite number

of higher-frequency optic-like modes should appear at the BZ. The relaxation frequencies of these higher-frequency modes which originate from the neighboring BZ are typically one order of magnitude higher than the relaxation frequency of the two lowest modes and can be neglected in view of their small contribution to the response of the system.

The contributions of the acoustic-like and lowest lying optic-like mode to the electrooptic response of a distorted helicoidal structure can be calculated from the free-energy density, which includes the electric polarization terms (Eq. (3)). This analysis can be simplified by considering the ***electric polarization properties of the phason excitations*** at the edge of the BZ. The relation between the fluctuation of the tilt order parameter $\boldsymbol{\xi}(z,t)$ and the polarization $\mathbf{P}(z,t)$ can be derived from the free-energy expansion (Eq. (4))

$$\delta P_x = \epsilon\mu \frac{d\delta\xi_x}{dz} - \epsilon C\, \delta\xi_y\,, \tag{76a}$$

$$\delta P_y = \epsilon\mu \frac{d\delta\xi_y}{dz} + \epsilon C\, \delta\xi_x\,. \tag{76b}$$

The space-averaged spontaneous polarizations $\langle \mathbf{P} \rangle$ of each mode at the edge of the BZ that are relevant for the linear response of the system at $q = 0$ are:

$$\text{The acoustic mode}: \quad \langle \delta P_x \rangle \propto \epsilon C \langle \mathrm{cn}^2(u,k) \rangle \neq 0\,, \tag{77a}$$

$$\langle P_y \rangle = 0\,. \tag{77b}$$

$$\text{The optic mode}: \quad \langle \delta P_x \rangle = 0\,, \tag{78a}$$

$$\langle \delta P_y \rangle \propto \epsilon C \langle \mathrm{sn}^2(u,k) \rangle \neq 0\,. \tag{78b}$$

Because the magnetic field is applied in the $y$-direction, we observe from the above equations that the acoustic mode represents a collective excitation with $\langle \mathbf{P} \rangle \perp \mathbf{H}$, whereas for the optic mode $\langle \mathbf{P} \rangle \parallel \mathbf{H}$. The above relations thus enable a selective probing of either the optic or the acoustic-like mode via the polarization-selective rules.

## References


1. S. A. Pikin and V. L. Indenbom, *Uspekhi Fiz. Nauk* **125**, 251 (1978).
2. R. Blinc and B. Žekš, *Soft Modes in Ferroelectrics and Antiferroelectrics* (North Holland, Amsterdam, Oxford, 1974).
3. R. M. Hornreich, M. Luban and S. Shtrikman, *Phys. Rev. Lett.* **35**, 1678 (1975).
4. A. Michelson, *Phys. Rev. Lett.* **39**, 464 (1977); *Phys. Rev.* **B16** 577 (1977); *Phys. Rev.* **B16**, 585 (1977).
5. L. Benguigui and A. E. Jacobs, *Ferroelectrics*, **84**, 379 (1988); A. E. Jacobs and L. Benguigui, *Phys. Rev.* **A39**, 3622 (1989).
6. B. Kutnjak-Urbanc and B. Žekš, *Phys. Rev.* **E48**, 455 (1993).

7. P. G. de Gennes, *Sol. State Comm.* **6** 163 (1968); R. B. Meyer, *Appl. Phys. Lett.* **12**, 281 (1968); G. Durand, L. Leger, F. Rondelez and M. Veyssie, *Phys. Rev. Lett.* **22** 227 (1969).
8. I. Muševič, B. Žekš, R. Blinc, Th. Rasing and P. Wyder, *Phys. Rev. Lett.* **48**, 192 (1982).
9. A. Seppen, Ph. D. Thesis, University of Nijmegen, The Netherlands (1987); see also R. Blinc, I. Muševič, B. Žekš and A. Seppen, *Physica Scripta*, **T35**, 38 (1991).
10. Z. H. Wang, Z. M. Sun and D. Feng, *Europhysics Lett.* **14**, 785 (1991).
11. I. Muševič, B. Žekš, R. Blinc, L. Jansen, A. Seppen and P. Wyder, *Ferroelectrics*, **58**, 71 (1984).
12. B. Žekš, *Mol. Cryst. Liq. Cryst.* **114**, 259 (1984).
13. T. Carlsson, B. Žekš, C. Filipič, A. Levstik and R. Blinc, *Mol. Cryst. Liq. Cryst.* **163**, 11 (1988).
14. N. A. Clark, and S. T. Lagerwall, *Appl. Phys. Lett.* **36**, 899 (1980); *Ferroelectrics* **59**, 25 (1984).
15. A. Golemme, S. Žumer, D. W. Allender and J. W. Doane, *Phys. Rev. Lett.* **61**, 2937 (1988); J. H. Erdmann, S. Žumer and J. W. Doane, *Phys. Rev. Lett.* **64**, 1907 (1990).
16. X-l. Wu, W. I. Goldburg, M. X. Liu, and J. Z. Xue, *Phys. Rev. Lett.* **69**, 470 (1992); N. A. Clark, T. Bellini, R. M. Malzbender, B. N. Thomas, A. G. Rappaport, C. D. Muzny, D. W. Schaefer and L. Hrubesh, *Phys. Rev. Lett.* **71**, 3505 (1993).
17. H. Hsiung, Th. Rasing and Y. R. Shen, *Phys. Rev. Lett.* **57**, 3065 (1986); W. Chen, L. J. Martinez-Miranda, H. Hsiung and Y. R. Shen, *Phys. Rev. Lett.* **62**, 1860 (1989).
18. S. A. Pikin, and K. Yoshino, *Jap. J. Appl. Phys.* **20**, L557 (1981); K. Kondo, H. Takezoe, A. Fukuda and E. Kuze, *Jap. J. Appl. Phys.* **21**, 224 (1982); K. Kondo, H. Takezoe, A. Fukuda, E. Kuze, K. Flatischer and K. Skarp, *Jap. J. Appl. Phys.* **22**, L294 (1983); S. Kai, M. Nakagawa, Y. Narushige and M. Imasaki, *Jap. J. Appl. Phys.* **22**, L488 (1983); Y. B. Yang, T. Bang, A. Mochizuki and S. Kobayashi, *Ferroelectrics* **121**, 113 (1991); M. Yamashita, *J. Phys. Soc. Jpn.* **52** 3735 (1983); M. Yamashita, *Ferroelectrics*, **58**, 149 (1984).
19. T. Povše, I. Muševič, B. Žekš and R. Blinc, *Liq. Cryst.* **14**, 1587 (1993).
20. M. Luban, D. Mukhamel and S. Shtrikman, *Phys. Rev.* **A10**, 360 (1974).
21. M. Glogarova, L. Lejček, J. Pavel, V. Janovec and J. Fousek, *Mol. Cryst. Liq. Cryst.* **91**, 305 (1983); M. Glogarova, J. Fousek, L. Lejček and J. Pavel, *Ferroelectrics*, **58**, 161 (1984); M. A. Handschy and N. A. Clark, *Ferroeletrics* **59**, 69 (1984); L. Bourdon, J. Sommeria and M. Kléman, *J. Phys. (Paris)*, **43**, 77 (1982).
22. V. A. Belyakov and V. E. Dmitrenko, *Optics of Chiral Liquid Crystals*, Soviet Scientific Review/Section A, Vol. 13, Part 1 (Harwood Academic Publishers), and the references therein.
23. M. A. Peterson, *Phys. Rev.* **A27**, 520 (1983).
24. C. Oldano, *Phys. Rev. Lett.* **53**, 2413 (1984).
25. I. Muševič, B. Žekš, R. Blinc and Th. Rasing, *Phys. Rev.* **E47**, 1094 (1993).
26. J. Goldstone, A. Salam and S. Weinberg, *Phys. Rev.* **127** 965 (1962); S. A. Bludman and A. Klein, *Phys. Rev.* **131**, 2364 (1963); R. V. Lange, *Phys. Rev.* **146**, 301 (1966); D. Forster, *Hydrodynamic Fluctuations, Broken Symmetry and Correlation Functions*, Frontiers in Physics (W. A. Benjamin, 1975).
27. L. van Hove, *Phys. Rev.* **95**, 1374 (1954). See also P. C. Hohenberg and B. I. Halperin, *Rev. Mod. Phys.* **49** 435 (1977) and the references therein.
28. L. D. Landau and I. M. Khalatnikov, *Dokl. Akad. Nauk. SSSR*, **96**, 469 (1954).
29. R. Blinc and B. Žekš, *Phys. Rev.* **A18**, 740 (1978). See also Ph. Martinot-Lagarde and G. Durand, *J. Phys. (Paris)*, **42**, 269 (1981).

30. L. Benguigui, *J. Phys. (Paris)*, **43**, 915 (1982).
31. S. Garoff and R. B. Meyer, *Phys. Rev. Lett.* **38**, 848 (1977); S. Garoff and R. B. Meyer, *Phys. Rev.* **A19**, 338 (1979).
32. A. Levstik, T. Carlsson, C. Filipič, I. Levstik and B. Žekš, *Phys. Rev.* **A35**, 3527 (1987); Ch. Bahr and G. Heppke, *Liq. Cryst.* **2**, 825 (1987); Ch. Bahr, G. Heppke, and N. K. Sharma, *Ferroelectrics*, **76**, 151 (1987); A. Levstik, T. Carlsson, C. Filipič, and B. Žekš, *Mol. Cryst. Liq. Cryst.* **154**, 259 (1988); C. Filipič, T. Carlsson, A. Levstik, B. Žekš, R. Blinc, F. Gouda, S. T. Lagerwall and K. Skarp, **A38**, 5833 (1988); A. M. Biradar, S. Wróbel, and W. Haase, *Phys. Rev.* **A39**, 2693 (1989); S. U. Vallerien, F. Kremer, H. Kapitza, R. Zentel and W. Frank, *Phys. Lett.* **138**, 219 (1989); T. Carlsson, B. Žekš, C. Filipič and A. Levstik, *Phys. Rev.* **A42**, 877 (1990).
33. I. Muševič, R. Blinc, B. Žekš, C. Filipič, M. Čopič, A. Seppen, P. Wyder and A. Levanyuk, *Phys. Rev. Lett.* **60**, 1530 (1988); I. Drevenšek, I. Muševič and M. Čopič, *Phys. Rev.* **A41**, 923 (1990).
34. I. Muševič, R. Blinc, B. Žekš, M. Čopič, M. M. Wittebrood, Th. Rasing, H. Orihara and Y. Ishibashi, *Phys. Rev. Lett.* **71**, 1180 (1993).
35. H. Sun, H. Orihara and Y. Ishibashi, *J. Phys. Soc. Jpn.* **60**, 4175 (1991); H. Sun, H. Orihara, and Y. Ishibashi, *J. Phys. Soc. Jpn.* **62**, 2066 (1993).
36. I. Muševič, B. Žekš, R. Blinc, H. A. Wierenga and Th. Rasing, *Phys. Rev. Lett.* **68**, 1850 (1992) and the reference therein.
37. I. Muševič, B. Žekš, R. Blinc and Th. Rasing, *Phys. Rev.* **B49**, 9299 (1994) and the references therein.
38. L. D. Landau and E. M. Lifshitz, *Quantum Mechanics*, 2nd edition (Pergamon, Oxford 1958).
39. B. Sutherland, *Phys. Rev.* **A8**, 2514 (1973).
40. A. D. Bruce and R. A. Cowley, *J. Phys. C: Sol. State Phys.* **11**, 3609 (1978).
41. B. J. Berne and R. Pecora, *Dynamic Light Scattering* (John Wiley, New York, 1976).
42. W. Kuczyński, B. Stryla, J. Hoffman and J. Malecki, *Mol. Cryst. Liq. Cryst.* **192**, 301 (1990); W. Kuczyński, J. Hoffmann and J. Malecki, to be published in *Ferroelectrics* (1994).